

A COMPARATIVE STUDY BETWEEN AXIAL AND RADIAL FLUX-
FOCUSING MAGNETIC GEAR TOPOLOGIES AND MECHANICAL GEARBOXES

by

Matthew Calvin

A thesis submitted to the faculty of
The University of North Carolina at Charlotte
in partial fulfillment of the requirements
for the degree of Master of Science in
Applied Energy and Electro-Mechanical Systems

Charlotte

2015

Approved by:

Dr. Wesley Williams

Dr. Jonathan Bird

Dr. Aidan Browne

©2015
Matthew Calvin
ALL RIGHTS RESERVED

ABSTRACT

MATTHEW CALVIN. Comparative study between flux-focusing magnetic gears and mechanical gears (Under the direction of DR. WESLEY WILLIAMS).

A variety of magnetic gear topologies have been investigated in recent years as alternatives to traditional mechanical gearboxes. In general these magnetic gears offer advantages in the non-contact transmission of torque including inherent overload protection, reduced acoustic emissions, and a reduction in the number of contacting components subject to wear. The earliest magnetic gear designs however suffered from low volumetric torque densities, which limited their utility for industrial applications. Research into flux focusing magnetic gearbox topologies has resulted in increased volumetric torque densities by actively engaging all of the magnets in the transmission of torque throughout the process. This research compared the volumetric torque density of axial and radial flux focusing magnetic gearbox designs and prototypes to planetary, cycloidal, and harmonic mechanical gearboxes. The rare earth scaled up radial and axial flux focusing topologies were found to have consistently higher volumetric torque densities than planetary gearboxes of comparable diameter. The cycloidal and harmonic gearboxes had comparable volumetric torque densities, with greater volumetric torque densities for some models and lesser volumetric torque densities for others. The expectation is that further improvements in volumetric torque density are possible for flux focusing magnetic gears with additional refinement and optimization of the designs. The current study does show that flux focusing magnetic gear topologies are a plausible future alternative to mechanical gearboxes in applications where their unique torque transmission mechanism would be advantageous.

ACKNOWLEDGMENTS

I would like to thank Dr. Wesley Williams for the many hours that he has spent working with me throughout the process of this thesis. I would also like to thank Dr. Jonathan Bird as my funding professor through undergraduate school and graduate school. I would also like to thank Dr. Aidan Browne for serving on my committee. I can't thank my mom and dad enough for supporting me throughout school along with my friends.

TABLE OF CONTENTS

| | |
|--|----|
| CHAPTER 1: INTRODUCTION | 1 |
| 1.1: Magnetic Gearbox Overview | 2 |
| 1.2 Objectives and Scope | 4 |
| CHAPTER 2: LITERATURE REVIEW | 6 |
| 2.1 Mechanical Gearbox History | 7 |
| 2.1.1 Planetary Gearbox | 9 |
| 2.1.2 Cycloidal Gearbox | 10 |
| 2.1.3 Harmonic Gearbox | 11 |
| 2.2 Magnetic Gearbox History | 12 |
| 2.2.1 Radial Magnetic Gearbox | 13 |
| 2.2.2 Axial Magnetic Gearbox | 17 |
| CHAPTER 3: METHOD | 19 |
| 3.1 Magnetic Gear Design | 19 |
| 3.2 Radial Flux Magnetic Gear Prototypes | 23 |
| 3.3 Axial Flux Magnetic Gearbox Prototypes | 26 |
| 3.4 Mechanical Gearbox Analysis | 26 |
| 3.4.1 Tooth Profiles | 28 |
| 3.4.2 Planetary Gearbox Design | 29 |

| | |
|--|----|
| 3.4.3 Cycloidal Gearbox Design | 32 |
| 3.4.4 Harmonic Gearbox Design | 34 |
| 3.4.4.1 Geometry of the Pitch Curve | 34 |
| 3.4.5.1 Finite Element Analysis Studies | 38 |
| 3.4.5.2 Magnetic Gear Mechanical Features Optimization | 39 |
| 3.4.5.3 Magnetic Gear Mesh Generation | 39 |
| 3.4.5.5 Magnetic Gear Fixtures | 42 |
| 3.4.5.6 Hybrid of FEA and Hand Calculation Method | 43 |
| 3.4.5.7 Magnetic Gear Optimization | 45 |
| 3.4.5.8 MG Mechanical Component Selection Analysis | 46 |
| 3.4.5.9 Axial Magnetic Gear Prototype Test Results | 53 |
| 3.5 Expected Results | 53 |
| CHAPTER 4: RESULTS | 55 |
| 4.1 Mechanical Gearbox | 55 |
| 4.1.1 Cycloidal Mechanical Gearbox | 57 |
| 4.1.2 Harmonic Mechanical Gearbox | 59 |
| 4.1.3 Planetary Mechanical Gearbox | 60 |
| 4.2 Magnetic Gearbox Testing | 62 |
| 4.3 Summary of Results | 65 |
| CHAPTER 5: CONCLUSION AND FUTURE SCOPE | 66 |

| | |
|--------------------------------------|-----|
| | vii |
| 5.1 Overview | 66 |
| 5.2 Recommendations and Future Scope | 68 |
| REFERENCES | 70 |
| APPENDIX: GEARBOX RAW DATA | 73 |

CHAPTER 1: INTRODUCTION

A magnetic gear (MG) is a device that provides a contactless mechanism for speed amplification or reduction. MGs only require bearing lubrication as opposed to mechanical gearboxes where gear lubrication is often also required. Another major advantage of a MG is that it has an inherent overload protection due to the absence of physical contact points between teeth, as in mechanical gearboxes. The rare earth magnets, which are frequently used in MGs, are very durable during MG overload; pole slipping is not likely to produce permanent damage, whereas in a mechanical gearbox an excessive overload will damage the mechanical gearbox (Cheng-Chi, Mi-Ching, Dorrell, & Bor-Jeng, 2008) . There is a tradeoff for the inherent overload protection, which is the torsional stiffness when compared to mechanical gearboxes (Frank, 2011). Due to the overload protection, various topologies of MG have been researched in recent years with a consideration of multiple applications. Even with the spike in interest, there has been relatively little published in the area of MGs in order to bring the technology to maturity (Frank, 2011).

To effectively evaluate flux-focusing, where the flux flows through steel poles, MGs for applications that have traditionally fallen to mechanical gearboxes, there is a need for a comparison between the flux-focusing MGs and commercially sold mechanical gearboxes. In addition, a standard way to compare flux-focusing MGs with mechanical gearboxes is desirable to be able to give designers the ability to determine

which type of gearbox is more advantageous for their project. Having a method to make a comparison between flux-focusing MGs and mechanical gearbox will improve the ability to compare the two. A flux-focusing MG that has been built along with mechanical gearbox data that is comparable by torque density, rated torque, gear ratio, volume, mass, and geometry will show the ability to be compared to commercially available mechanical gearboxes. The MGs were tested through the range of operating conditions.

1.1 Magnetic Gearbox Overview

A MG, shown in Figure ,1 consists of p_1 pole-pair permanent magnets, referred to as PMs, that can rotate at ω_1 , a middle rotor with n_2 ferromagnetic steel poles that are able to rotate at ω_2 , and p_3 pole-pair PMs that rotate at ω_3 (V. M. Acharya, Bird, & Calvin, 2013). The inner and outer rotors contain ferromagnetic pieces along with permanent magnets. On these rotors there are usually a large difference between the number of poles on the inner (high speed) and outer rotor (fixed/low speed). The magnets on these rotors are commonly surface-mounted magnets for many of the configurations that have been proposed. Surface-mounted magnets are expensive and as such, the MG being studied uses rectangular magnets that are less costly. In general, the layouts of MGs are borrowed directly from layouts intended for mechanical gears (Frank, 2011). The MGs looked at are shown in the Table 1, showing when the paper for each of the MGs were published along with topology and magnet type.

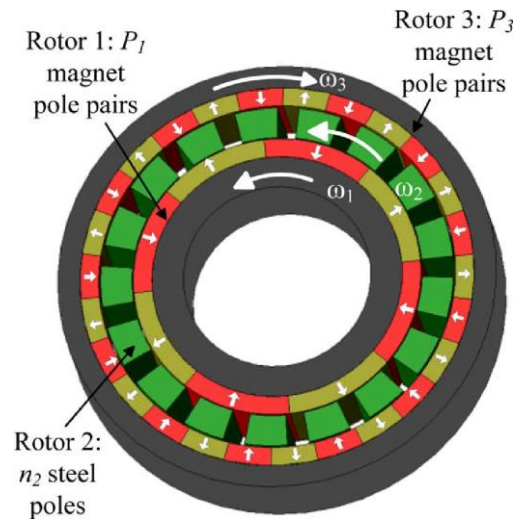


Figure 1: Surface-mounted radial MG layout(V. M. Acharya et al., 2013)

Table 1: Historical list of magnetic gearboxes

| Author | Date | Configuration/ Topology | Magnet Type |
|--------------|------|----------------------------|---|
| Atallah | 2001 | Coaxial | Rare-earth-permanent |
| Bronn | 2012 | Axial | Rare-earth-permanent |
| Faus | 1941 | Gear-pair | Ferrite-permanent |
| Hesmondhalgh | 1980 | Coaxial-multi stage | Electro-magnet |
| Laing | 1972 | Coaxial | Ferrite-permanent using flux modulation pieces in magnet rotors |
| Martin | 1968 | Radial | Ferrite-permanent |
| Mezani | 2006 | Axial | Rare-earth-permanent |
| Neuland | 1916 | Coaxial | Electro-magnet |
| Rasmussen | 2005 | Coaxial | Rare-earth-permanent |
| Reese | 1967 | Coaxial | Ferrite-permanent |
| Tsuruimoto | 1987 | Axial spur gear | Rare-earth-permanent |

1.2 Objectives and Scope

An axial flux-focusing magnetic gearbox (AFFMG) topology is predicted to be able to achieve higher active region torque densities than the radial equivalent, however, this is yet to be experimentally verified (V. M. Acharya et al., 2013). There has yet to be a comparison of torque densities and torque ripple of an AFFMG gear and conventional mechanical gears (i.e. spur gears, planetary gears, etc.). Such a comparison would give insight into application abilities and show the application advantages of an AFFMG.

There are several aspects to be considered in a comparison of AFFMG and mechanical gearboxes to determine which is needed for an application. This can be done with comparing torque densities by volume, torque densities by mass and torque ripple. The method of using torque density by volume is done by examining the gearbox to determine the active torque transfer volume of the gearbox and then using the rated torque of the gearbox to calculate torque per volume. The torque density by mass is calculated by taking the rated torque divided by total mass of the gearbox. The torque ripple is the fluctuation in torque transfer of a gearbox, playing a key role in the performance of the gearbox, due to many machines needing steady torque input. One of the key requirements for increased torque transfer in MGs is controlling the air-gap; where the air-gap is the distance between magnetically interacting rotors, giving the contactless torque transfer.

For long life applications, MGs could offer a much longer service life due to their contactless torque transfer capability and only requiring bearing lubrication. Another possible application for MGs is under uncertain loading circumstances that can arise from highly variable loads, such as shock loading. MGs have greater resilience in these

conditions than mechanical gearboxes, again due to the contactless torque transfer, which allows the poles to slip without causing any mechanical failures. However control approaches need to be utilized in order to allow the gearbox to recover from one pole slippage condition.

In a planetary gearbox there are limiting factors, for example, gear ratio limitations in planetary gears, such as having a maximum and minimum number of teeth that are able to be used. There are also few options for overload protection when using a mechanical gearbox; typically the mechanical gearbox is either oversized or has another mechanical system to govern the torque being input into the gearbox. This leads to inefficiencies, an increase in cost, and reliability issues.

CHAPTER 2: LITERATURE REVIEW

Historically, mechanical gearboxes are considered the standard in torque transfer and industry has been content in using the mechanical planetary or epicyclical gears for torque transfer. There have been significant advances in power production, but little done to improve the method for the transfer of torque. The oversizing of mechanical gearboxes for shock loading increases the mass and volume that has to be incorporated into the overall design, which can become a large hindrance for producing large scale energy production equipment such as wind turbines and current turbines. In horizontal wind turbines it is advantageous to have a gearbox that has less mass due to the difficulty of having a large mass at a high elevation being supported by a thin beam.

As stated previously, a MG has an inherent overload capability; this capability does not require a magnetic gearbox to be oversized to be able to handle the overload conditions. Magnetic gears require less maintenance than their mechanical gearbox counterparts, which is advantageous for ocean energy current turbines due to the difficulty for maintenance on current turbines being deep under water. MGs have typically used large quantities of rare earth magnets, with the emerging technology of adding ferromagnetic pole pieces uses flux-focusing arrangements (K. Uppalapati & Bird, 2012).

There are many other applications where an axial flux MG is advantageous due to the configuration of equipment. One example is in helicopters, where axial flux MG

could reduce the issues of alignment of the axial MG rotors and gives a relatively short axial length gearbox. Another example of a possible application is in the use of vertical axis wind mills. The advantage for using an axial MG on vertical wind mill is much like the helicopter where a short axial length requires less volume for the MG. There are limited publications detailing axial MGs, therefore their torque densities and construction requirements are not well understood. Acharya's paper states that the evaluated design would give relatively high volume torque densities in excess of 250 Nm/L while having a relatively small torque ripple (V. M. Acharya, Calvin, & Bird, 2014).

2.1 Mechanical Gearbox History

Three different types of gearboxes: planetary, cycloidal and harmonic, are reviewed in this thesis, with the individual advantages and disadvantages of each being examined. Mechanical planetary gearboxes first appeared in ancient China around 2600 BC in a device called the south-pointing chariot, a two-wheeled vehicle with a pointer set to south that would point south however the chariot moved (Corey, 2003). Afterwards, the mechanical gearbox went largely unnoticed through human history for approximately 2500 years until it was shown to be useful as a calculator for predicting eclipses and other astrological events, with a particular example being the Antikythera machine in ancient Greece (Corey, 2003). Cycloidal and harmonic gearboxes are known as a wobble gearbox due to the gearboxes having an internal eccentric portion that produces an orbital path or 'wobble'. The first of these wobble gearboxes was patented in 1895 by Daniel Regan, shown in Figure 2 (Regan, 1895). In Figure 2, labels A and D create the eccentric portion of the gearbox while C, B and E are the meshing gears.

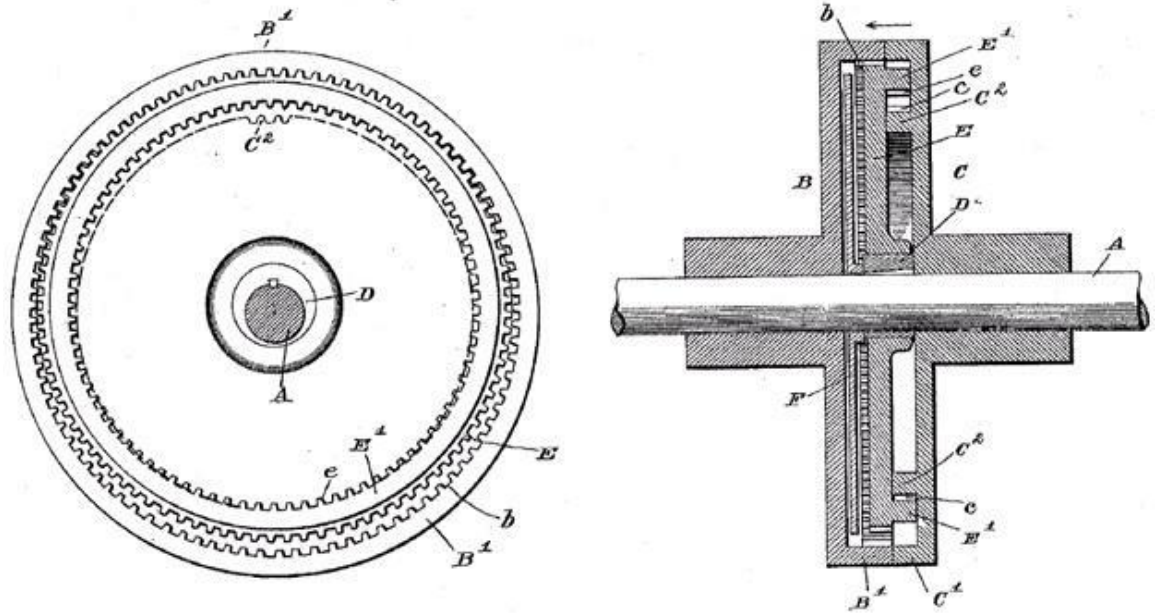


Figure 2: The first wobble gearbox created by Regan in 1895, where it introduced a slight eccentric, shown in A and D(Regan, 1895)

The first cycloidal gearbox was created by De la Hire, Poncelet, and Camus (Litvin & Lewis Research, 1997). These gearboxes were initially used in watches (Litvin & Lewis Research, 1997). Cycloidal gearboxes were desired in watches due to the gearboxes having a small amount of backlash, which occurs when there is a small gap between teeth surfaces that are not engaged.

An important part of torque transfer is efficiency; losses from use of gearboxes in a complete transmission can cause other components, such as shafts and bearings in, the system to be oversized to be able to compensate for the low efficiency and still meet the torque transfer requirements. The efficiency of mechanical gearboxes can range from 50% efficiency to greater than 98% efficiency depending on geometry and configuration as shown in Table 2 below.

Table 2: Theoretical mechanical gears efficiency ranges (Mobley, 1999)

| Gear type | Efficiency Range (%) |
|---|----------------------|
| Bevel gear, hypoid | 90-98 |
| Bevel gear, miter | N/A |
| bevel gear, spiral | 97-99 |
| bevel gear, straight | 97-99 |
| bevel gear, zerol | N/A |
| helical gear, external | 97-99 |
| helical gear- double , external (herringbone) | 97-99 |
| spur gear, external | 97-99 |
| worm, cylindrical | 50-99 |
| worm, double-enveloping | 50-98 |

2.1.1 Planetary Gearbox

The planetary gearbox is used successfully in applications that range from rotary storage to planetary motion and torque transfer. A planetary gearbox includes four main components as is shown in Figure 3. The components are: the sun gear, which is in the center of the gearbox, the planets which are located around the sun, and can vary from having one to nine planets, the carrier which holds the planets while also being able to rotate (not shown in Figure 3) and the ring gear which encompasses the three other components. Not until the 1841 publication of Willis's *Principles of Mechanisms* was an attempt made to create an analytical model of the gearbox. Since Willis's analytical model there have been a large number of studies done on designing planetary mechanical gears giving rise to some of the most common gearbox applications. Even though there

have been relatively few published papers that investigate torque densities of a planetary gearbox, with a focus toward torque density as a method of optimization.

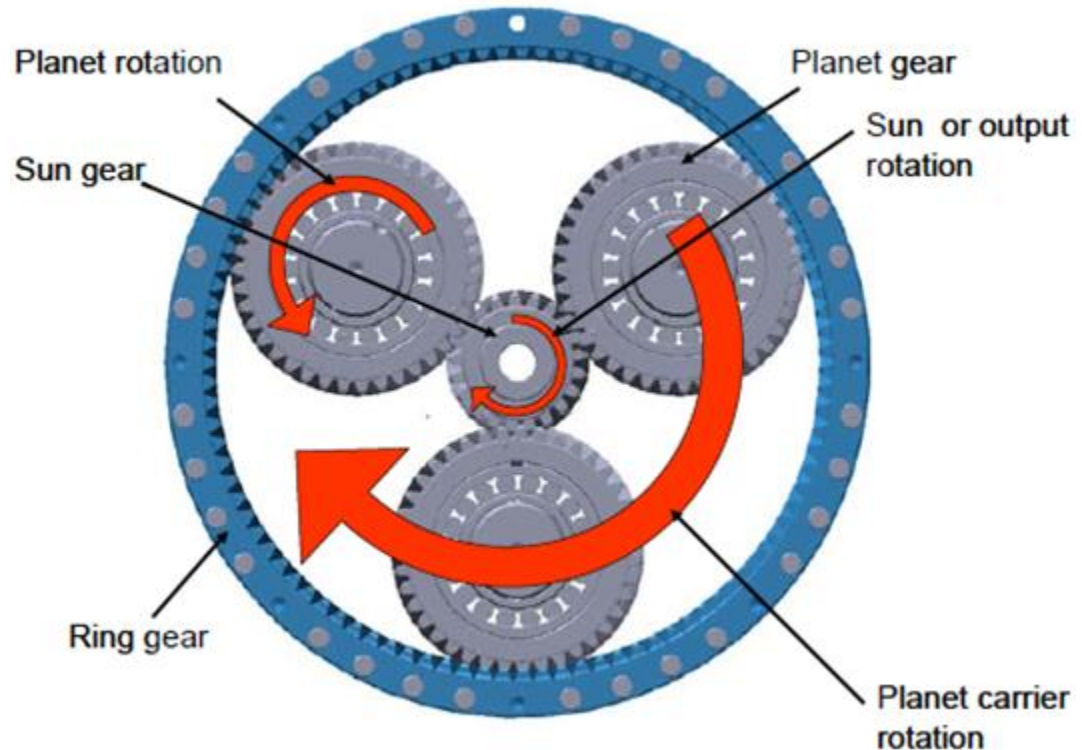


Figure 3: Planetary gearbox diagram showing three of the four main components of a planetary gearbox, sun, planets, carrier, and ring, while also showing the rotational pattern of each(Oyague, 2009)

2.1.2 Cycloidal Gearbox

The proper name for a cycloidal gearbox is hypocycloidal gearbox when used in gear transmission configuration; the hypocycloidal name comes from the tooth profile design. A cycloidal gearbox is comprised of four parts: the cycloid disk, eccentric, pins and rollers, as seen in Figure 4. Figure 4 shows a simple cycloidal gearbox, having only a single stage. The eccentricity is the reasoning for it being classified under the wobble gearbox category. Cycloidal gearboxes have large gear ratios that can range from 6:1 up to 120:1. A notable feature is that this can be accomplished with a single stage of gears

(Crowder, 2006). The cycloidal gearbox is also noted for having high stiffness and low backlash (Crowder, 2006).

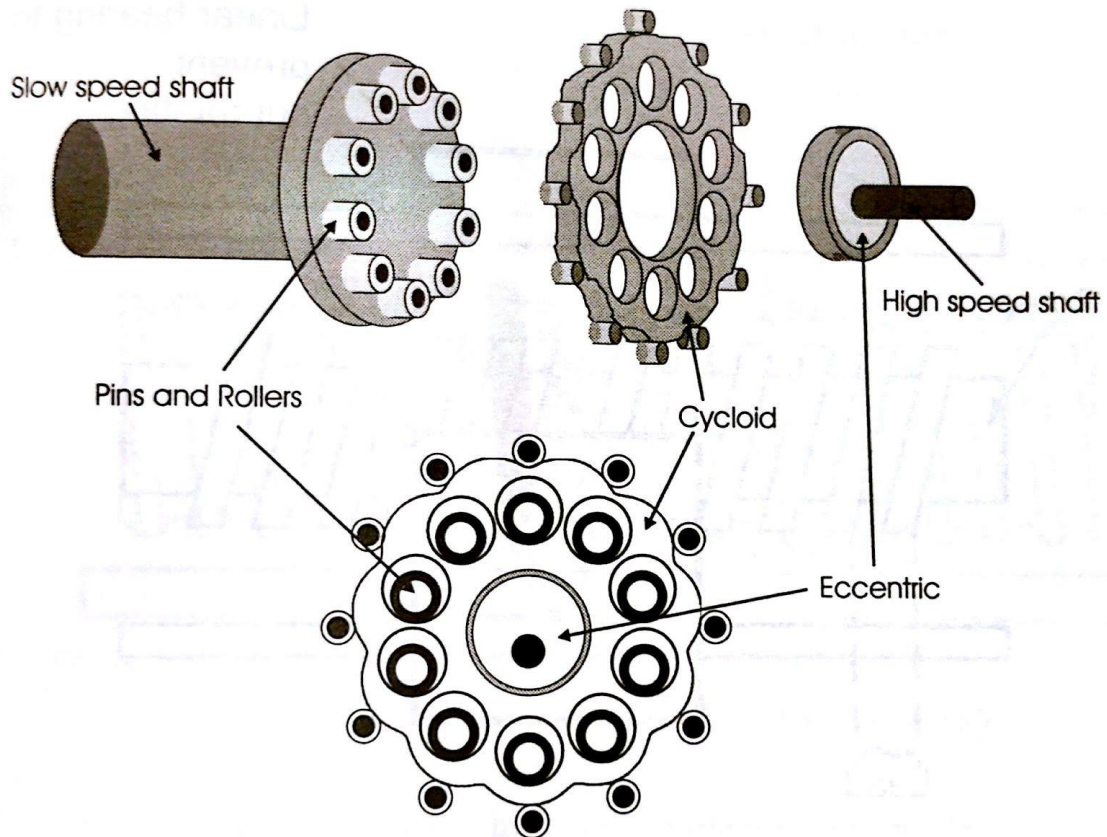


Figure 4: Cycloidal gearbox diagram showing the four main components and the input and output shafts (Crowder, 2006)

2.1.3 Harmonic Gearbox

The harmonic drive, also known as the strain wave gearing, was first applied in aircraft and defense applications and was invented by Walt Musser in 1959 (Ueura & Slatter, 1999). There are three main components of a harmonic gearbox: the circular spline, flex spline and the wave generator shown in Figure 5. The harmonic gearbox operates by turning the wave generator, which is an elliptical shape, which causes the flex

spline to distort outwards causing it to mesh with the circular spline. The gear ratios of a harmonic gearbox are available from range 3:1 up to 120:1. The first published aerospace application of a harmonic gearbox was in 1971, this was used as the transmission element within each individual wheel drives of the Lunar Roving Vehicle on the Apollo 15 mission. The harmonic gearbox has almost zero backlash which allows the gearbox to have constant drive in both directions. Another major advantage of the harmonic gearbox in aerospace applications is that it does not require lubricant, which is a critical attribute in the freezing vacuum of space (Bronn, 2012; Ueura & Slatter, 1999).

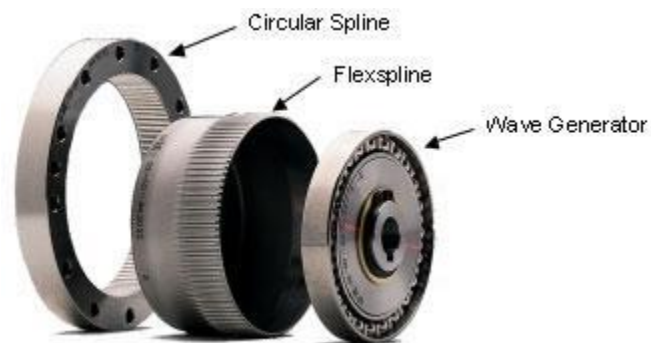


Figure 5-Harmonic gearbox assembly, this shows that the flex spline is smaller than the circular spline and that the wave generator does not have teeth ("Operating Principles," 2015)

2.2 Magnetic Gearbox History

Neuland filed a patent in 1916 for an electromagnetic geared system similar to Figure 1; the main difference from that figure is that only one member contained a magnetized winding, the fixed rotor (K. K. Uppalapati, Bird, Dan, Garner, & Zhou, 2012). The concept of a gearbox using permanent magnets dates back as early as the 1940's with a US patent by Faus shown in Figure 6 (Frank, 2011). These early MGs used ferrite magnets in a spur gear configuration and yielded poor torque densities when compared to

a mechanical gear (Frank, 2011). The early MGs yielded low torque capabilities due to the topology of the magnets; Faus's a topology resembles a mechanical gear pair. This design did not have overload capability due to the magnets meshing like the teeth of a gearbox.

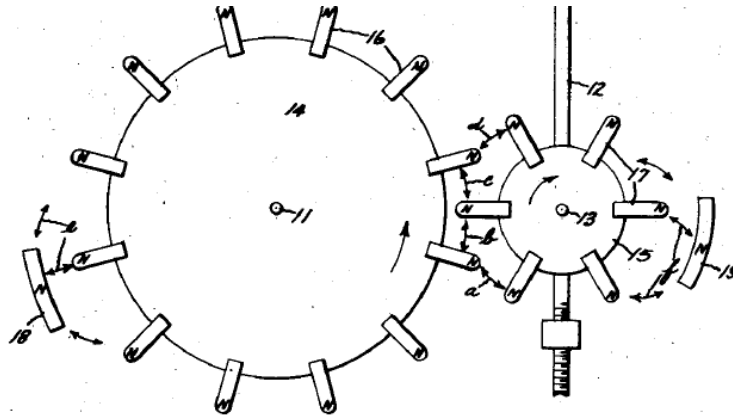


Figure 6: Faus's permanent magnet MG with no overload protection (Faus, 1941)

As noted previously, MG's have an inherent overload protection but if the maximum torque is exceeded the input speed must be reduced to approximately zero to allow the MG to re-engage. Bronn stated this in his experimental results and has also been found true during the testing done on the MGs at The University of North Carolina at Charlotte (UNCC) (Bronn, 2012; Neuland, 1916).

2.2.1 Radial Magnetic Gearbox

Radial MGs are more commonly known as coaxial MGs, this research refers to radial MG as such due to the flux flow. Radial MGs have been studied more thoroughly than their axial MG counterpart. The radial MG publications dating as far back as 1916 with one of the first by Neuland, as stated previously (Neuland, 1916). In 1967 Resse created a similar design to Neuland only the inner rotor contained permanent magnets. In Resse's design the outer rotor was kept stationary while the middle rotor and inner rotor

were allowed to rotate. The inner rotor was the high speed side and the middle rotor was the low speed side; this configuration is shown in Figure 7 (Reese, 1967). In Reese's design the magnetic flux of the permanent magnets usually takes the path with the least permeability, which was through the steel teeth in the rotors. This caused the teeth of the rotor to rotate and the speed of the rotor became a function of the ratio of the number of teeth between the rotors and the number of permanent magnet poles (Bronn, 2012). Not long after Reese, Martin designed a similar MG in 1968, shown in Figure 8. Martin's design differed only by replacing the outer and inner rotor with permanent magnets while leaving the middle rotor having flux modulation pieces, labeled 28, this is shown in Figure 8 (Bronn, 2012). In this thesis the flux modulation pieces are referred to as the cage rotor in the radial MG of the UNCC designs as further detailed in Chapter 3.

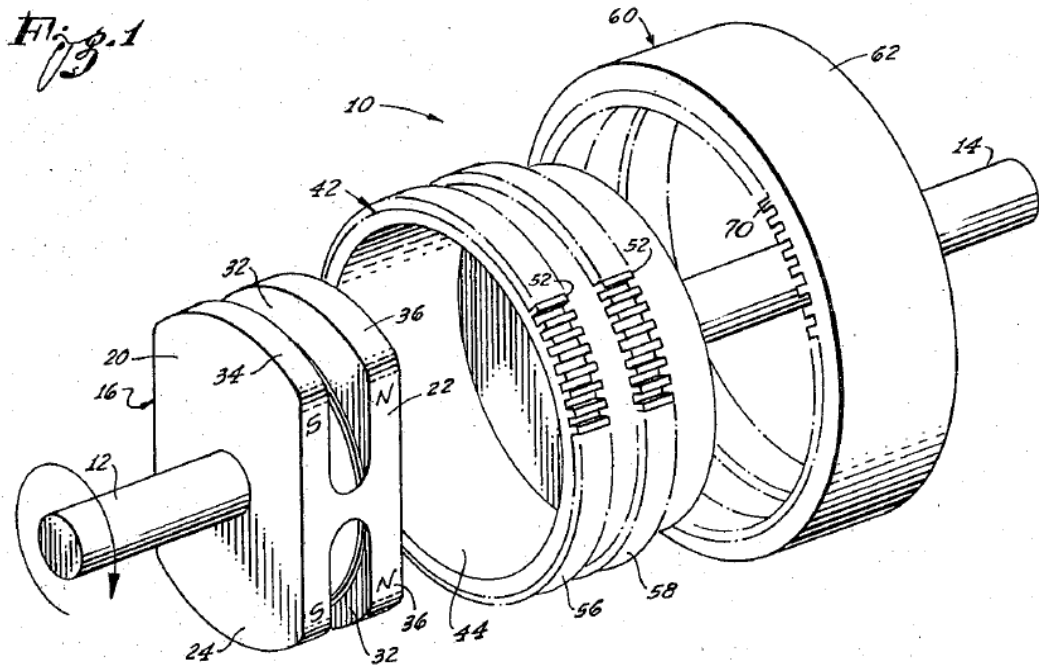


Figure 7: Reese coaxial design (Reese, 1967)

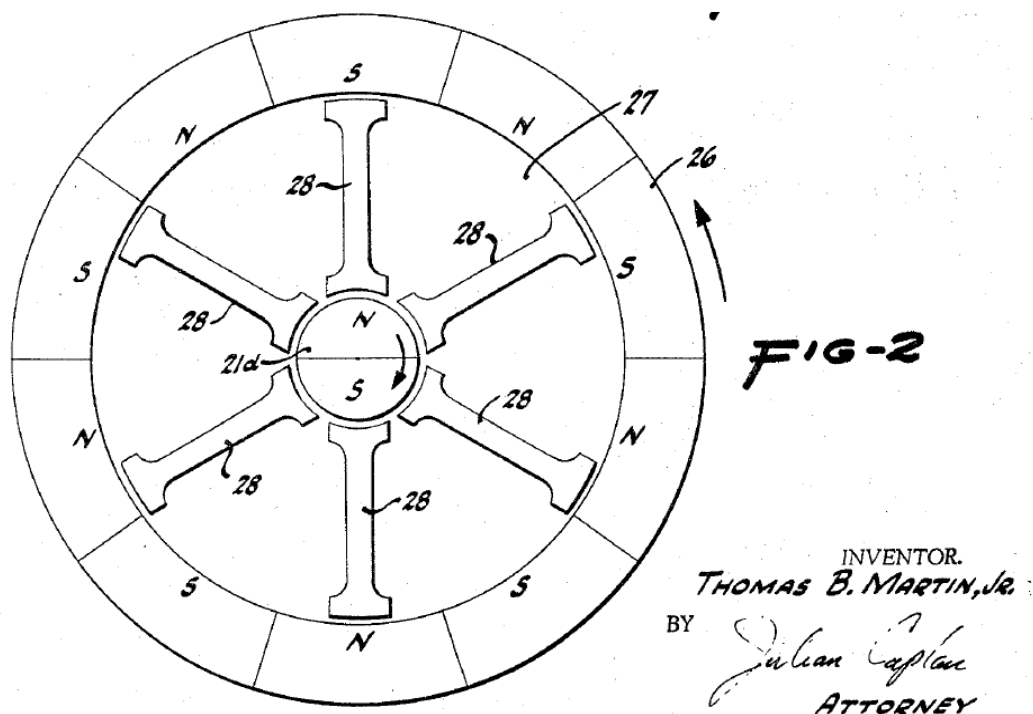


Figure 8-Martin coaxial design showing the flux modulations pieces between the inner and outer rotor magnets(Thomas, 1968)

In 1972 Laing was granted a patent for a MG that operated in a similar way to Martins shown in Figure 9, it differed only in the shape of flux modulators and also that every second pole on the rotor contained permanent magnets (Bronn, 2012). Laing later took out another patent in 1973 incorporating a MG into a centrifugal pump (Bronn, 2012; Hesmondhalgh & Tipping, 1980). In 1980, Hesmondhalgh proposed a series of Neuland's MGs to increase torque transmission and reduce the cogging torque (Hesmondhalgh & Tipping, 1980). The cogging torque is the amount of oscillation in torque transfer of the gearbox.

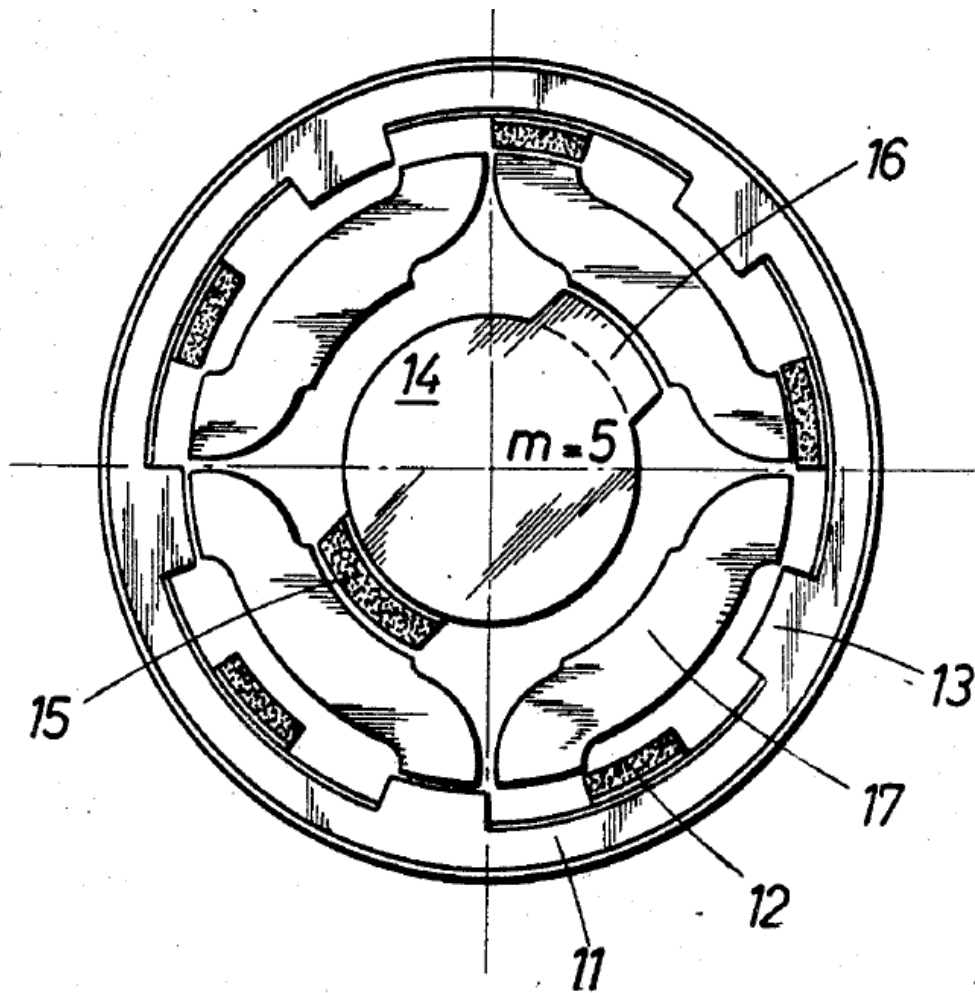


Figure 9-Laing's Coaxial Design(Nikolaus, 1972)

In 2001, Atallah designed a MG using rare earth magnets that was calculated to achieve a torque density that exceeded 100 kNm/m^3 . Rasmussen published a coaxial MG similar to Atallah's except that the inner rotor's magnets were arranged in a spoke-type arrangement and not surface-mounted magnets. Rasmussen's MG had a theoretical 27 Nm torque capability which gave a torque density by volume of 92 Nm/L along with a torque density by mass of 14.2 Nm/kg and a theoretical efficiency of 96%. The experimental torque of Rasmussen's MG was 16 Nm. Rasmussen's MG yielded a torque

density by volume of 54 Nm/L and a torque density by mass of 8.4 Nm/kg while also yielding an efficiency of 81%.

2.2.2 Axial Magnetic Gearbox

One of the first proposed axial MGs was by Tsuruino in 1987 (Tsurumoto & Kikuchi, 1987). Tsuruino's MG was comprised of two non-equal sized disks configured in a spur gear type configuration as shown in Figure 10 (Tsurumoto & Kikuchi, 1987). In 2006 Mezani presented an axial MG using surface-mounted magnets with a gear ratio of 5.75:1 and a 200 mm diameter with a torque density of 70 Nm/L. While in 2010 Hirata presented a surface mounted axial MG with a higher gear ratio of 10:1, a 120 mm diameter and a torque density of 19 Nm/L (V. M. Acharya et al., 2013).

It is generally accepted that axial flux motors can generate a higher torque density than their radial counterparts (V. M. Acharya et al., 2013). This is due to the assembly constraints in the radial configuration not allowing the rotors to be the same length. Bronn proposed and tested an axial MG with an air-gap of 4 mm capable of no load input torque of 200Nm which gave an active torque density of 37.7kNm/m^3 (Nm/L) and a torque ripple of 8.7% each of which were slightly higher than the simulated values of 195.85Nm, an active torque density of 35kNm/m^3 and a torque ripple of 4.9%. Bronn's design had low efficiencies of only 35% at 50rpm, due to much higher losses in the design than what was simulated. The simulated efficiency was 69.4% at 50rpm. Bronn stated that the axial flux MG that was tested was the first of which was experimentally evaluated. In Bronn's thesis it also states the difficulty of the axial flux topology due to the axial forces being primarily in one direction. The axial forces do not fully counter each other like the radial forces do in a radial flux MG (Bronn, 2012). Bronn also states

in the paper that there had been little mechanical optimization of the gearbox that was produced and experimentally tested. While there was some Finite Element Analysis (FEA) performed, no optimization was performed. Unlike their radial counterparts, AFFMGs have not been studied at great length, driving the research interest in the Laboratory for Electromechanical Energy Conversion and Control at UNCC. In this thesis the flux modulation pieces are referred to as the spoke rotor in the AFFMG of the UNCC designs as further detailed in Chapter 3.

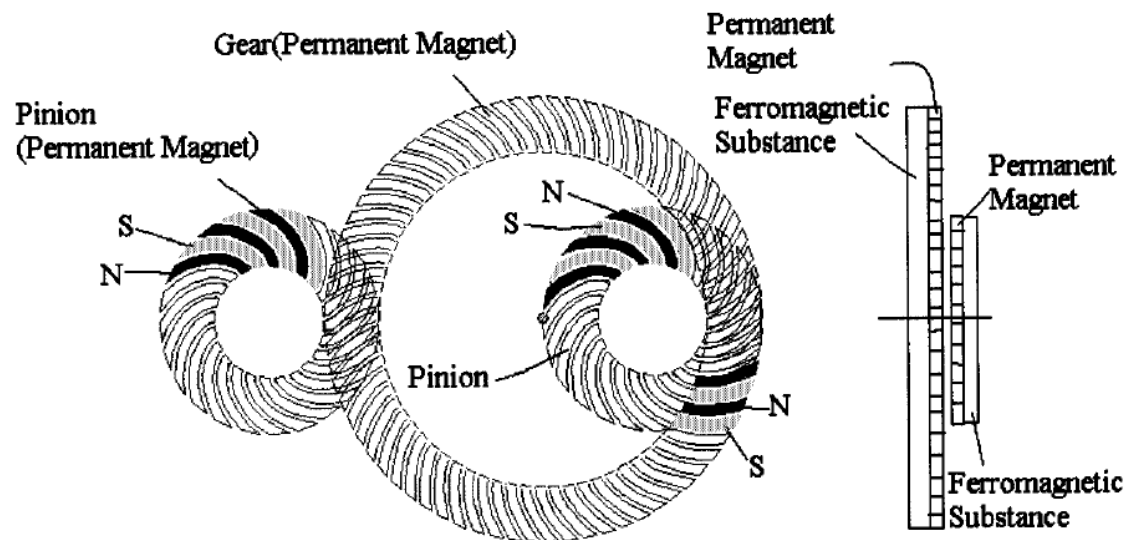


Figure 10: Tsurumoto's Axial MG design using a two rotor helical topology (Tsurumoto & Kikuchi, 1987)

CHAPTER 3: METHOD

An AFFMG has been assembled and tested at UNCC in the Electrical and Computer Engineering department. The AFFMG has been mounted to a test bed to measure the torque capabilities along with torque ripple and was tested to assess the performance relative to the proposed specifications and initial simulations for the axial MG. With the testing complete, a comparison between the AFFMG and three types of mechanical gearboxes was made in relation to their torque-per-unit-mass along with the torque per unit volume, efficiency, and prediction of failure modes. This comparison of flux-focusing MGs and mechanical gearboxes is a method to compare the two types of gearboxes, this has been completed to simplify the analysis of possible applications of the two types of gearbox.

3.1 Magnetic Gear Design

The primary factors in the design of a gearbox are its dimensions, velocity ratio, and maximum transmission torque (Cheng-Chi et al., 2008). When analyzing MGs a higher least common multiple for the fixed stator operation has the effect of lowering the torque ripple; this is due to the cogging torque factor being closer to one (Gouda, Mezani, Baghli, & Rezzoug, 2011). The cogging torque factor determines the cogging torque and the torque ripple. Increasing the number of pole pairs on the high speed rotor will decrease the torque ripple as stated by Frank, but this is limited due to the number of pole pairs on the fixed rotor, which is ultimately limited because of the difficulty of

manufacturing continually smaller magnets along with the ferromagnetic pieces (Frank, 2011). Frank also stated that the gear ratio along with the layout of the magnets played a key role in the torque ripple associated with a given configuration (Frank, 2011). Unlike the radial flux focusing counterpart, the predicted torque ripple has been observed to be relatively high for AFFMGs when comparing to radial flux focusing counterpart (V. M. Acharya et al., 2013). Although, the recent testing of the AFFMG exhibited low torque ripple.

The relationship between the poles is chosen so as to cause the rotors to interact through a common space harmonic component(V. M. Acharya et al., 2013).

$$p_1 = |p_3 - n_2| \quad (1)$$

Such that p_1 represents the number of pole pairs on the high speed rotor, p_3 represents the number of pole pairs on the fixed rotor, and n_2 represents the number of ferromagnetic pole pieces on the low speed rotor.

The approach taken by Acharya to maximize torque density with a given configuration is to hold two of the three rotor's axial length constant while varying the length of the other rotor(V. M. Acharya et al., 2013). This approach is shown in Figures 11 through Figure 13; the figures show how the axial length of each rotor changes the torque density of both volume and specific torque density. When using this approach with ferrite magnets the maximum volume torque and mass torque density of 60 Nm/L and 14 Nm/kg occurred when the axial length is $l_{s1} = 40$ mm for the high speed rotor shown in Figure 12 (V. M. Acharya et al., 2013). When this process was repeated for the ferromagnetic steel pole rotor, the axial thickness of 9.5 mm was found to give a peak volume and mass torque density of 65 Nm/L and 5.5 Nm/kg respectively as shown in

Figure 13, further details are given in (V. M. Acharya et al., 2013). The volume used to determine the volume torque density was the encompassing volume of the gearbox.

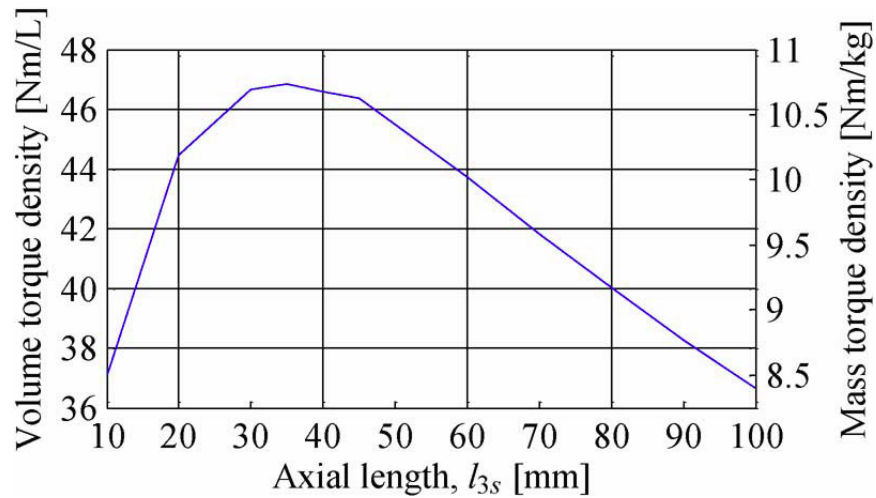


Figure 11: Torque density with respect to the axial length of the fixed rotor (l_{3s}) on the axial MG (V. M. Acharya et al., 2013)

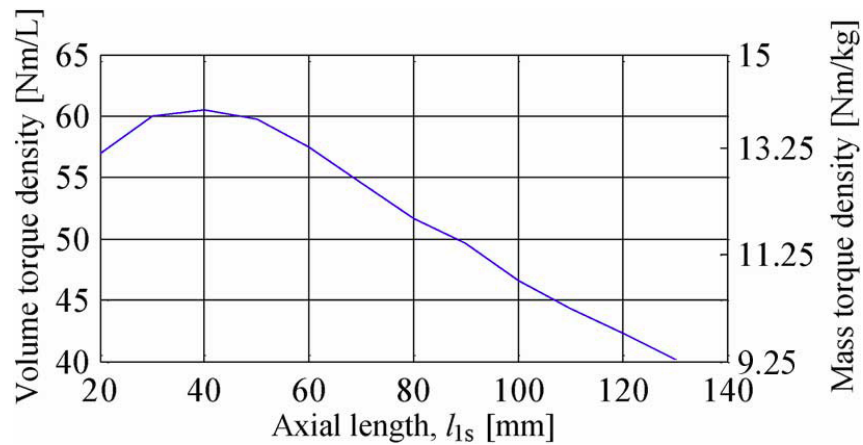


Figure 12: Torque density with respect to the axial length of the high speed rotor (l_{1s}) on the axial MG (V. M. Acharya et al., 2013)

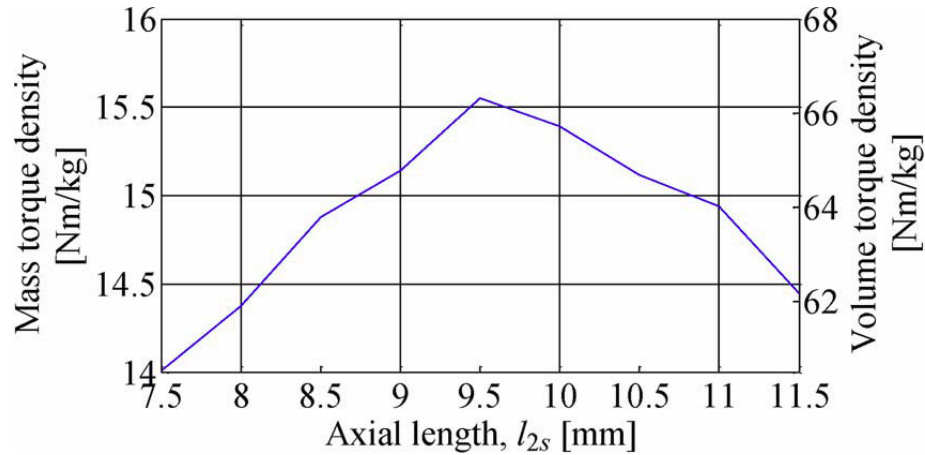


Figure 13: Torque density with respect to the axial length of the spoke rotor (l_{2s}) on the axial MG (V. M. Acharya et al., 2013)

The angular rotational velocities for each rotor of the MG are related by

$$\omega_1 = \frac{p_3}{p_3 - n_2} \omega_3 + \frac{n_3}{n_2 - p_3} \omega_2 \quad (2)$$

The gear ratio equation is simplified when rotor 3 is assumed to be stationary

$$\omega_1 = \left(\frac{n_2}{p_1} \right) \omega_2 = G_{12} \omega_2 \quad (3)$$

Using (3) with a pole combination of $p_1=7$, $n_2=22$, Acharya obtained a gear ratio of $G_{12}=3.14$ (V. M. Acharya et al., 2013). Gouda indicated that a low gear ratio has a higher torque density for MGs (K. K. Uppalapati et al., 2012). MGs that have whole gear ratios offer the worst performance followed by MGs with half and third ratios, other fractional ratios offered the best performances as stated by Frank, which gives an opportunity to improve performance of an MG (Frank, 2011). According to Frank, having what is referred to as the high speed rotor fixed is not considered due to its low gear ratio (Frank, 2011).

A measure, suggested by Gouda, to increase flux density was to have a smaller air-gap between rotors. With an increase in the flux density that was caused by the

reduction of the air-gap between the rotors the torque was also increased. Gouda suggested this after doing the analysis using an air-gap of 2 mm (Gouda et al., 2011). The air-gap studied at UNCC is 0.5 mm. Due to the low RPM values being used in this thesis the hysteresis losses are assumed to be negligible, but the eddy current loss can still be high due to the usage of solid steel bars (V. M. Acharya et al., 2013; K. K. Uppalapati et al., 2012).

3.2 Radial Flux Magnetic Gear Prototypes

Dr. Jonathan Bird's Laboratory for Electromechanical Energy Conversion and Control at UNCC currently has two working prototypes for a radial flux-focusing MG. Included in these two prototypes are several other design variants, including using a soft magnetic composite as the cage rotor, replacing the cage rotor with steel laminations, and adding a stator rotor to the scaled up design to give a constant variable radial MG. The process for designing the ferrite magnet radial flux MG active region was designed by creating an inner rotor with a given number of pole pairs which was then used along with the number of outer rotor pole pairs to determine the optimal magnet thickness. The results of the analysis completed by Uppalapati are shown in Figure 14 (K. Uppalapati & Bird, 2012). As the torque increases for the outer rotor magnet thickness increases and the torque density increase till a thickness of 14 mm where the torque density begins to decline as shown in Figure 14.

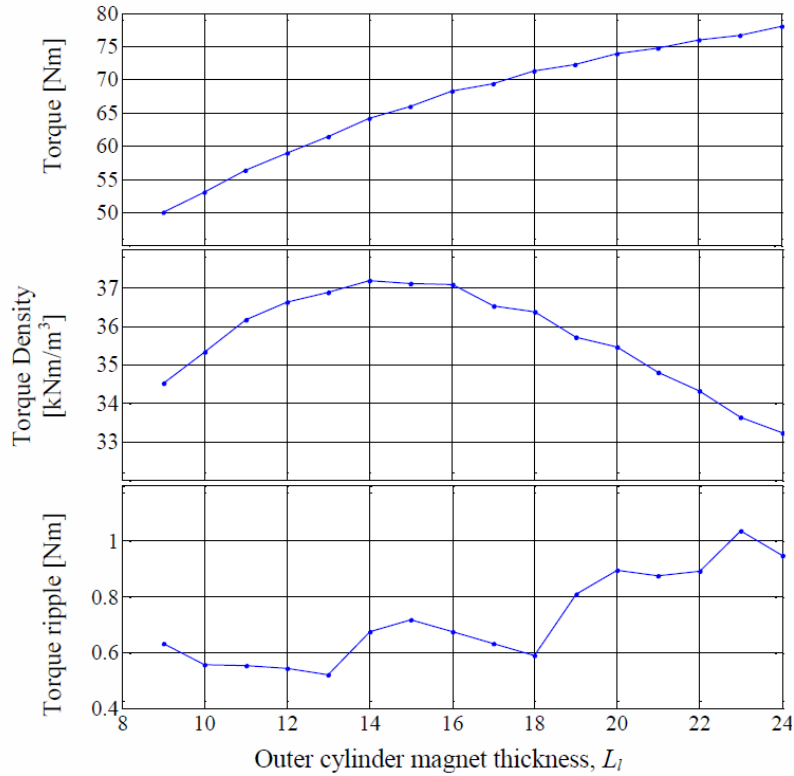


Figure 14: Outer rotor magnet thickness for a ferrite magnet design (K. Uppalapati & Bird, 2012)

The results from the outer cylinder analysis and the previously set number of steel bars for the cage rotor were then used to determine the thickness and width of the cage rotor steel pieces. The results can be seen in Figure 15 and 16, that were created by Uppalapati (K. Uppalapati & Bird, 2012). As the radial thickness of the cage rotor steel pieces increases until 10 mm where it begins to level, where the maximum torque density is found to be at 6 mm. As the angular width of the cage rotor steel pieces continues to increase the torque density increases along with the torque values, this continues until 15 mm.

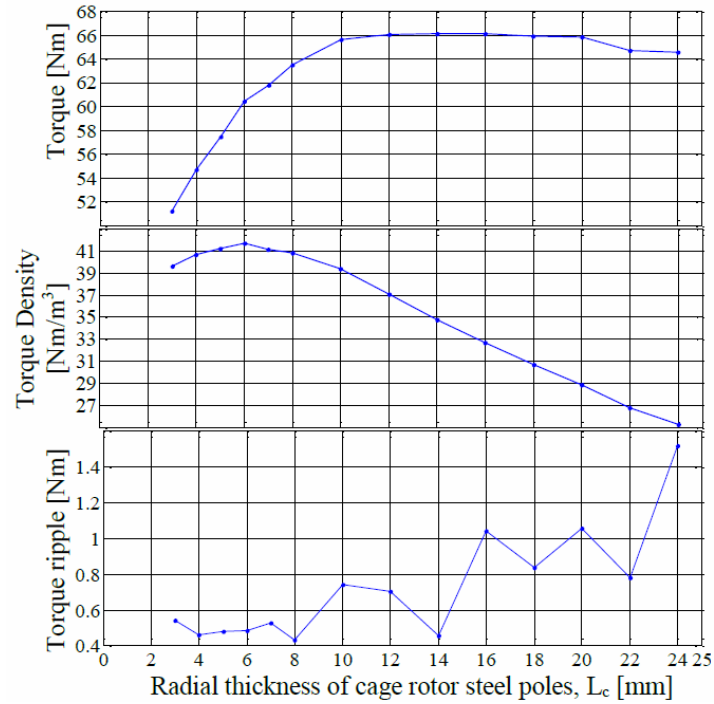


Figure 15: Analysis radial thickness of cage rotor steel poles for the ferrite magnet design (K. Uppalapati & Bird, 2012)

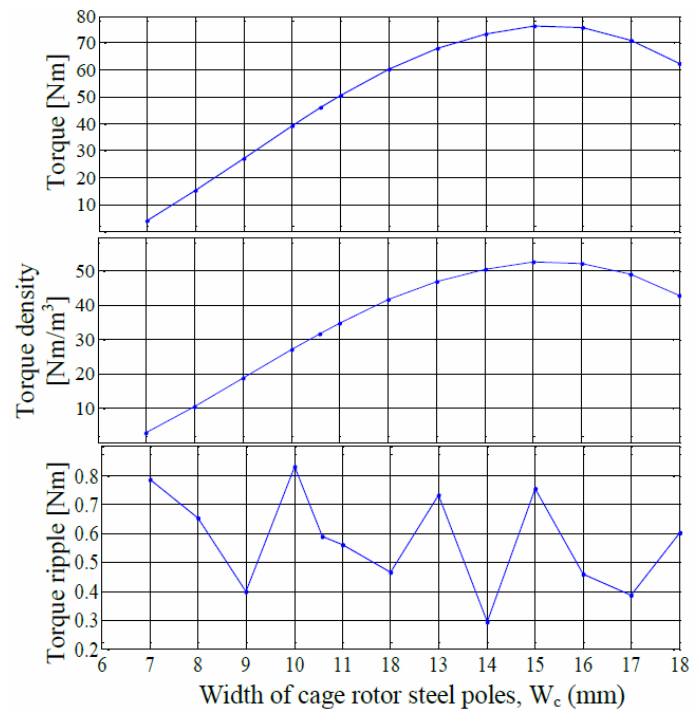


Figure 16: Analysis of angular width of cage rotor steel poles for the ferrite magnet design (K. Uppalapati & Bird, 2012)

3.3 Axial Flux Magnetic Gearbox Prototypes

Frank encountered several problems when assembling a prototype of a radial flux MG. The first of which was the concentricity between the inner and outer rotors; it was pointed out that a key difficulty in the construction and assembly of rotor 2 was the maintaining of the air-gap on both sides of the ferromagnetic pieces (Frank, 2011). These challenges have led to only a few working prototypes being successfully manufactured. UNCC currently has a working AFFMG. The magnetic design was completed by Vedanadam Mudumbai Acharya while the mechanical features were designed by the author (Vedanadam Mudumbai Acharya, 2013). As the AFFMG is the first prototype built at the University, there are significant opportunities for further optimization in the mechanical design.

3.4 Mechanical Gearbox Analysis

The process for determining the volume torque density was analyzed in several steps. The initial process started by taking the largest cylinder the gearbox could fit into and calculating the volume of this bounding cylinder. With this non-essential volume removed the gearbox is then assumed to be a series of disks. Having the series of disks simplified the volume calculation and granularity can be increased easily by adding more disks to closely match the features of the gearbox. Subsequent calculations were made using stacks of cylinders to account for the variation in diameter with axial position in order to refine the granularity of the volume calculation, shown in Figure 17. This has been completed for several gearbox manufacturers along with several models of gearboxes from each manufacturer. This process excluded shafts and mounting plates from this calculation, which is the same as in the MG calculations. The types of

mechanical gearboxes that were analyzed for their torque densities are epicyclic, harmonic, and cycloidal.

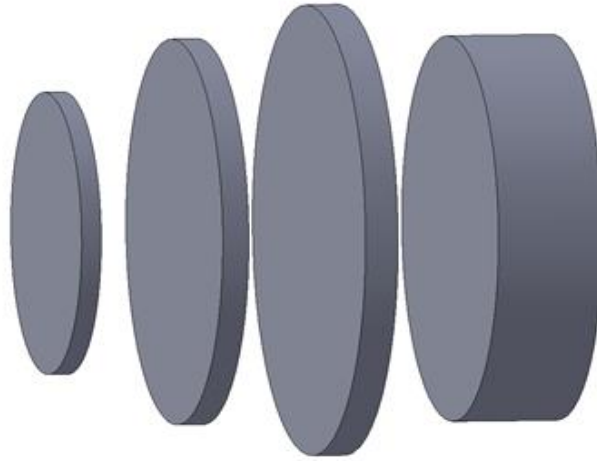


Figure 17: Cycloidal gearbox volume analysis cylinder diagram exploded view. Showing cylinder arrangement, demonstrating the removal of non-active region of the gearboxes

The three most common types of failure for a epicyclic (planetary) gearbox are tooth breakage, pitting of teeth, and scoring (Spotts, Shoup, Hornberger, & Kazmer, 2004). Tooth breakage may be caused by unexpectedly heavy loads on the teeth or from bending fatigue, which is caused by many repetitions of loading imposed on the tooth as the gear rotates. The failure mode of pitting occurs when the stresses exceeds the endurance limit of the surface material. Failure by pitting often occurs by many loading cycles which cause small bits of material to fatigue and dropout. This increases rapidly due to there being less non-pitted areas to carry the load. Pitting failures can also be caused by lubrication difficulties in a planetary gearbox. Failure due to scoring can occur while under heavy loads and inadequate lubrication; having inadequate lubrication during heavy loading can also cause the oil film to break down and causing metal-to-metal

contact. Metal-to-metal contact causes heat and when high temperatures are present two surfaces in contact can weld together and then immediately break; this causes rapid wear. Scoring happens mostly on coarse pitched teeth, fine pitch teeth are largely immune to scoring (Spotts et al., 2004).

3.4.1 Tooth Profiles

The standard tooth profile for a planetary and a harmonic gearbox is an involute tooth profile. A simplified approach to creating an involute curve is to wrap a string tightly around a circle and connecting a pen to the end of the string, while keeping the string tight and tangent to the circle an involute curve will be created much like the one shown in Figure 18.

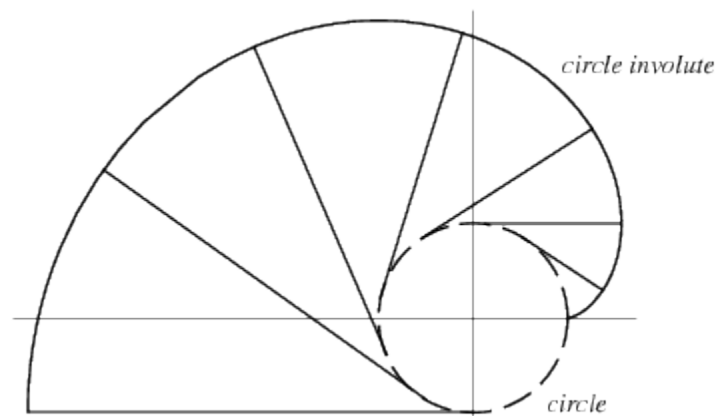


Figure 18: Circle involute curve that creates a tooth profile, area in which the teeth a gearbox mate (Weisstein)

Diametral pitch is the number of teeth, N , in the gear per length of pitch diameter, d , the equation for determining diametral pitch, P_d

$$P_d = \frac{N}{d} \quad (4)$$

The circular pitch is defined from a point on the pitch circle of one tooth to the corresponding point on the adjacent tooth measured along the pitch circle.

The tooth profiles of the cycloidal gearbox disk are in a cycloidal curve shape. The conceptual design of a cycloidal disk can be done by tracing a point inside of a generating circle as it rolls around a base circle (Sensinger, 2010). The procedure for doing this can be seen in Figure 19. Where R_g is the generating circle, R_p is the radius of the base circle, R is the offset of the rollers and e is the eccentricity of cam.

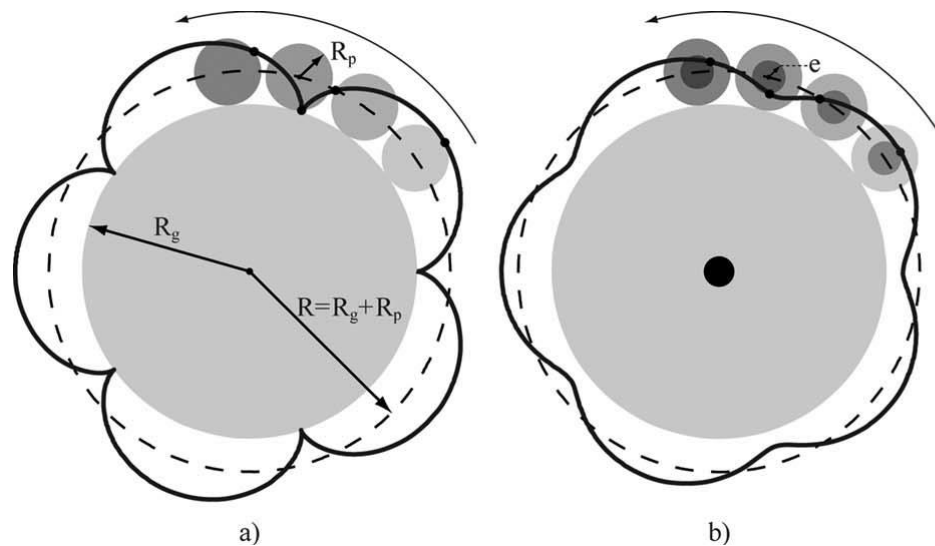


Figure 19: a) shows how the cycloidal profile may be visualized by tracing a point on a generating circle as it rolls around a base circle b) shows a point inside of the generating circle to avoid undercutting (Sensinger, 2010)

3.4.2 Planetary Gearbox Design

For mechanical planetary (epicyclical) gearboxes the designer must select one torque, along with either three or two speeds and a gear ratio (Corey, 2003). With these parameters selected, there are two methods looked at for the analysis of a planetary gearbox using the American Gear Manufacturing Association (AGMA) method along with the Society of Automotive Engineers (SAE) method. Each of these methods uses

different factors and assumptions when designing gears. Both considered the Hertz stress on the gear along with the bending strength.

The starting point for planetary gearbox design is determining the gear ratio which is given by

$$G_{tf} = \frac{\text{number of driver gear teeth}}{\text{number of driven gear teeth}} \quad (5)$$

Once the gear ratio is determined the gearbox is designed to be sized to avoid bending or pitting failures. The equation for the bending strength, s_t , when using the AGMA method is:

$$s_t = \frac{W_t K_o K_v K_s P d}{F} \left(\frac{K_m K_b}{J} \right) \quad (6)$$

where W_t is the transmitted tangential load on the gear tooth. There are several safety factors involved in this calculation which are: K_o is the overload factor, K_v is the dynamic factor, K_s is the size factor, K_B is the rim thickness factor, K_m is the load distribution factor and J is the geometry factor for bending strength. The variable F in this equation is the face width. The equation for the pitting strength (hertz stress), S_c , when using the AGMA method is

$$S_c = c_p \sqrt{\frac{W_t K_o K_v K_m C_f}{d F I}} \quad (7)$$

where the variables are valid from the bending strength analysis. The variables unique to the AGMA pitting are c_p , which is the elastic coefficient, and C_f which is the surface condition factor for pitting resistance and I which is the geometry factor for pitting resistance. The equation for bending strength, s_t , when using SAE method is

$$s_t = \frac{W_t P d}{F J_{pinion}} \quad (8)$$

The equation for pitting strength (hertz stress) when using SAE method is

$$s_c = 0.59 \sqrt{\frac{FE}{L} \left(\frac{1}{d_1} + \frac{1}{d_2} \right)} \quad (9)$$

where E is the modulus of elasticity, L is the tooth width, and d_1 and d_2 are the diametral pitches of the two mating gears respectively. Willis' relation for a planetary mechanical gear is given by (10),

$$0 = k\Omega_1 + (1 - k)\Omega_4 - \Omega_3 \quad (10)$$

where k is the gear ratio and Ω is the rotational velocity of a specific gear (Gouda et al., 2011).

The safety factors are large drivers in the torque density of a planetary mechanical gearbox but when the safety factor becomes very low the service life comes into question (Gouda et al., 2011). These safety factors are difficult to determine because the factors are based on manufacturing experience along with the designer's input on what the factors should be for a given design. Corey stated that the principle of energy conservation can be used to analyze the torque on individual gears in a planetary gear train, giving a greater depth of knowledge in to analyzing the design of planetary gearboxes (Corey, 2003). The results due to excessive Hertz stress is shown in Figure 20

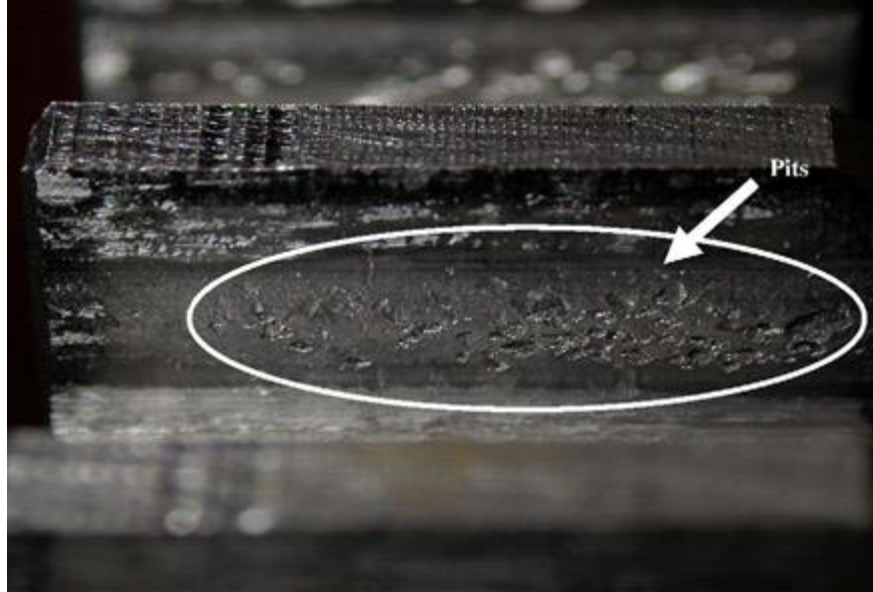


Figure 20: Example of Hertz (Pitting) fatigue on mechanical gear tooth flank(Tan, Irving, & Mba, 2007)

Planetary gearbox efficiency is determined by the mechanics of the design and is covered by the standard methods for spur gears (Tan et al., 2007). This considers how the tooth is engaged and if the specific gear has internal teeth or external teeth along with the mating gear.

3.4.3 Cycloidal Gearbox Design

Cycloidal gearboxes contain three main components: an input shaft, an output disk, and an intermediate disk that wobbles relative to the output disk.

The gear ratio equation for a cycloidal gearbox is,

$$GR = \omega_{input}/\omega_{output} = z_1/(z_2 - z_1) \quad (11)$$

where ω_{input} is the input shaft angular velocity and ω_{output} is the angular velocity of the output disk, z_1 is the number of cycloid lobes and z_2 is the number of rollers.

The cycloidal tooth profile C can be mathematically determined by using the equations that were derived by Shin and Kwon shown in (12) and (13) (Shin & Kwon, 2006). The shape of the cycloid profile along with the roller path is shown in Figure 21.

$$C_x = R \cos\phi - R_r \cos(\phi + \psi) - e \cos((z_1 + 1)\phi) \quad (12)$$

$$C_y = -R \sin\phi + R_r \sin(\phi + \psi) + e \sin((z_1 + 1)\phi) \quad (13)$$

where R is the offset of rollers, ϕ is the input angle, ψ is the contact angle, and e is the eccentricity of the cam. The contact angle, ψ , between the cycloid lobe and roller is calculated from

$$\psi = \tan^{-1} \left[\frac{\sin(Z_1\phi)}{\cos(Z_1\phi) - \frac{R}{e(Z_1+1)}} \right] \quad (14)$$

where ϕ is the angle of the input shaft. When designing cycloidal gearboxes it is necessary to ensure that undercutting, the excessive removal of material does not occur and that rollers do not intersect each other. The three following equations are able to check for undercutting (Sensinger, 2010).

$$R_{r \max} = \sqrt{27Z_1 \frac{[R^2 - e^2(Z_1+1)^2]}{(Z_1+2)^3}} \quad (15)$$

$$R_{\min} = \sqrt{\frac{R_r^2(Z_1+2)^3}{27Z_1} + e^2(Z_1+1)^2} \quad (16)$$

$$e_{\max} = \sqrt{\frac{27R^2Z_1 - R_r^2(Z_1+2)^3}{27Z_1(Z_1+1)^2}} \quad (17)$$

where R_r is the roller radius, $R_{r \max}$ is the maximum roller radius, R_{\min} is the minimum offset of the rollers, e_{\max} is the maximum eccentricity of the cam. The equation to check that the rollers are small enough so that they do not intersect each other is (Sensinger, 2010).

$$R_{r \max} = R \sin\left(\frac{\pi}{Z_1+1}\right) \quad (18)$$

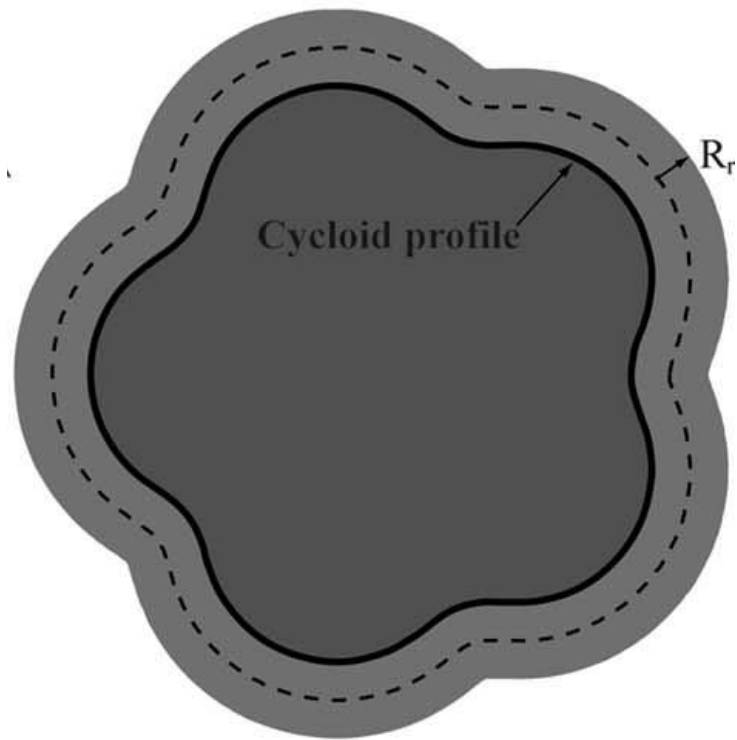


Figure 21: The cycloid profile(Sensinger, 2010)

3.4.4 Harmonic Gearbox Design

Harmonic gearboxes can be designed with pure involute tooth gear pairs. During the design process it is assumed that the gear tooth has sufficient rigidity so that it maintains its gearing property.

3.4.4.1 Geometry of the Pitch Curve

The center of the flex spline (pinion) will lie on a line QN at a distance of A from the y-axis, shown in Figure 22, where A is the center distance between the ring gear and the un-deflected pinion in the mesh and is calculated from (Maiti, 2004):

$$A = (Z_g - Z_p)m/2 \quad (19)$$

where Z_g and Z_p are the number of teeth on the ring gear and the flex spline respectively and m is the module, which is the ratio of pitch diameter in millimeters to the number of teeth. “For each point on the ellipse, the intersection of the radius of curvature with the line QN is determined”(Maiti, 2004). Then, the length along the radius of curvature is calculated; this is repeated until the length of the radius of curvature from the point of intersection, O_2 , becomes equal to the pitch circle radius of the pinion(Maiti, 2004). The ellipse in Figure 22 can be described with respect to the xO_1Y axis by the following equation:

$$\left[\frac{x}{a}\right]^2 + \left[\frac{y}{b}\right]^2 = 1 \quad (20)$$

Where $(x, y) = (x_1, y_1)$ are the coordinates with respect to the xO_1Y axes of the junction point ‘D’, in Figure 22, of the ellipse and the circular arc. The variable a in (20) is the semi major axis of the elliptical curve in proposed cam profile and b is the semi minor axis of the elliptical curve in proposed cam profile. The coordinates of the center of curvature ‘E’ of the ellipse are given by:

$$x_c = x_1^3 \left(\frac{a^2 - b^2}{a^4} \right) \quad (21)$$

$$y_c = y_1^3 \left(\frac{b^2 - a^2}{ba^4} \right) \quad (22)$$

The intersection of the radius of curvature with line $x=A$ with respect to the xO_1Y axes is given by the following:

$$c = y_1 - \left(\frac{y_1 - y_c}{x_1 - x_c} \right) (x_1 - A) \quad (23)$$

Where c is the shift of the major axis of ellipse from the central axis of the ring gear. The distance from O_2 to point D is known as l which is the radius of curvature of the ellipse at the junction of the elliptical curve with circular arc and is expressed as (24)

models for the active section were generated off of two-dimensional sketches that were generated from previous analysis completed in the magnetic simulation program JMAG. These three-dimensional models were then used to generate the mechanical features required to give structural support to the active magnetic section of the MG. The effect of the mechanical features on the magnetic performance had to be considered to make sure there was no short circuiting of the fields through the mechanical features. This was achieved by isolating all active regions from all of the inactive regions through adding plastic spacers, layers of plastic sheets, nonconductive paint, and anodizing aluminum parts. The 3D models include all mounting features and hardware that were used in an assembly; this is including all features that were to be used on the produced prototype. This was done to give the most accurate model analysis and representation to resemble the actual stresses established in the gearbox.

The material properties used during the finite element analysis were predefined in SolidWorks, and verified against values published in the MatWeb database ("MatWeb,"). These materials were assumed to be linearly elastic and isotropic. Setting these characteristics will assume that after the material is loaded that it will return to its original shape and zero stress point, based on the stresses staying lower than the elastic limit.

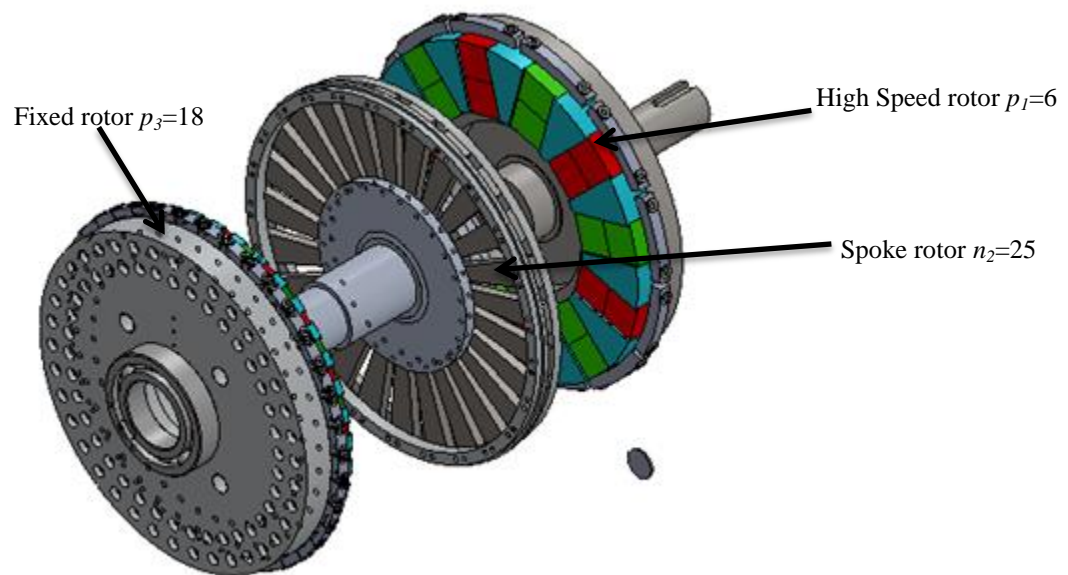


Figure 23: Axial flux-focusing magnetic gearbox compared to a coin (a U.S. quarter)

3.4.5.1 Finite Element Analysis Studies

Mechanical FEA was performed to give further insight into the mechanical feature stress analysis and optimization for the different MGs that have been designed and assembled at UNCC. The FEA software used during the analysis of these components was Dassault Systèmes SolidWorks Simulation module. The FEA data used for analysis can be seen in Table 3.

Table 3: Magnetic gear model FEA data

| Part Name | Simulation type | Nodes | Elements | Mesh | Boundary Conditions | Applied Load | Deflection |
|---------------------------------|-----------------|--------|----------|--|-----------------------------------|--|------------------|
| Cage rotor end plate shaft side | Static | 142144 | 92202 | Solid, curvature based, Jacobian points at nodes | Fixed in three direction(X, Y, Z) | Torque load(1600N-m) Pressure (700 N/m ²) | 0.02987 mm (max) |
| Cage rotor bar | Static | 11316 | 6817 | Solid, Standard, 4 points | Fixed in three direction(X, Y, Z) | Normal force (580 N) | 0.01769 mm (max) |
| Spoke rotor correction plate | Static | 33884 | 19762 | Solid Mesh, Standard, 4 points | Fixed in three direction(X, Y, Z) | Normal force (10000 N) | 0.04648 mm (max) |

3.4.5.2 Magnetic Gear Mechanical Features Optimization

The mechanical features of the MG were optimized using FEA. The simulations considered during this analysis were static loading, dynamic loading, and fatigue simulations. Using FEA results, excess material was removed by identifying stressed and unstressed locations in the loaded part. Once the stress values were calculated, the life of the mechanical features of the MG were then used to analyze if the life expectancy is comparable to its mechanical gearbox counterpart. The life expectancy was checked through FEA simulations along with using numerical hand calculations by using the Goodman line along with Basquins equation (Spotts et al., 2004). The desired life expectancy for mechanical gearboxes used in large wind turbines is approximately twenty years (Ragheb & Ragheb, 2010).

3.4.5.3 Magnetic Gear Mesh Generation

The mesh used during the FEA analysis of the magnetic gears was a modified standard mesh in SolidWorks. The modifications of the mesh were modified through using the mesh generator which was set to have automatic transitions between mesh sizes

and to have a mesh control setting an aspect ratio of 1.0. SolidWorks uses a tetrahedral 3D solid element for all solid components. This was done to give the smallest size elements in the smaller areas as possible, while in the larger areas the mesh was much larger due to there being less drastic changes in the these features; an example of this mesh generation is shown in Figure 24.

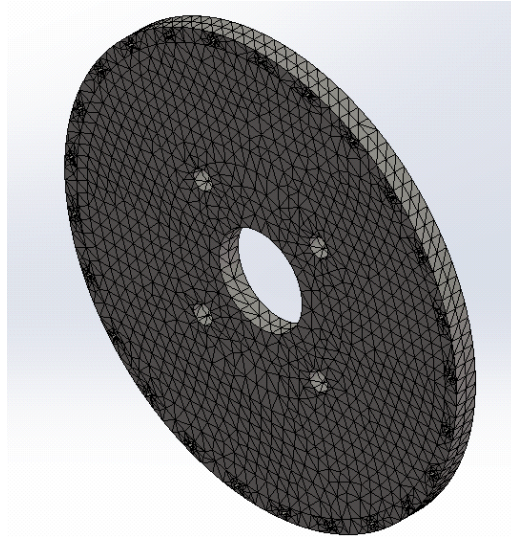


Figure 24: Axial MG correction plate model showing automatic transitions mesh

3.4.5.4 Magnetic Gearbox Loading

The MG loading was taken from previously performed magnetic analysis, computed by colleagues in the laboratory for Electromechanical Energy Conversion and Control, which gave the torque being transferred through the MG. The torque along with the magnetic forces that act on the active regions are transferred to the mechanical features. The forces were assumed to be constant, and based on the maximum values. The maximum values are then carried through to the cyclic loading, which is fully reversed loading. The forces that were being applied were assumed to be perpendicular to the faces, whereas the torque being applied was tangent to the face of the part. The

area being loaded is determined by the active magnetic region, along with the mounting surface due to using standard available parts for mounting.

During Bronn's minimal mechanical FEA work on the Axial MG, the simulations are shown to have comparatively large deflections but this was not a factor in Bronn's MG due to the air-gap being large (Bronn, 2012). Bronn also assumed that the forces were constant, which is not completely correct, due to the magnetic forces increasing as the rotor bar deflects and moves closer to the magnets. This assumption gives a reference to determine if the deflection of the rotor bars is significant or not. This was repeated for the spoke rotor of the AFFMG, first for the difference in the forces of the fixed and high speed rotor and assuming that the bars are fixed cantilever beams, which gave a very small deflection. This was found to be incorrect, because during assembly, the spoke rotor is exposed to unidirectional loading, which causes the spokes to deflect until contact is made with the other rotor. It was also found that the assumed fixed joint of the spoke rotor was not completely fixed. The unidirectional force loading caused the bolts, which were assumed to be fixed on the spoke rotor, were deflecting large enough to cause an angular displacement. With this angular displacement it causes an increase in the forces on the bars represented in Figure 25, which increased the deflection.

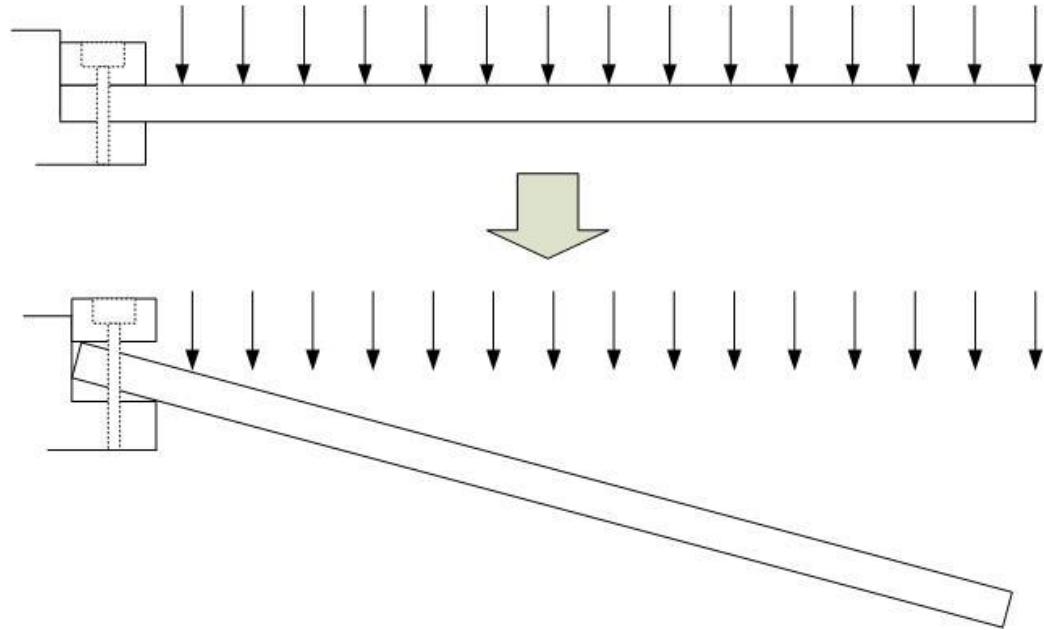


Figure 25: Spoke rotor deflection; top image is expected results from a fixed joint, lower picture is the actual result from mounting not being completely fixed

3.4.5.5 Magnetic Gear Fixtures

Typically to perform FEA, some regions must be fixed and these regions were determined based off of the torque transfer and magnetic loading. The fixture type used for analyzing the MG mechanical features is fixed in three directions. Fixing the mechanical parts in three directions allows for multiple loads to be analyzed, including loading due to the torque being transmitted, the loading due to magnetic forces on the steel bars, and the loading due to mounts and bearings. In Figure 26 the highlighted region shows an example of the assumed fixed geometry.

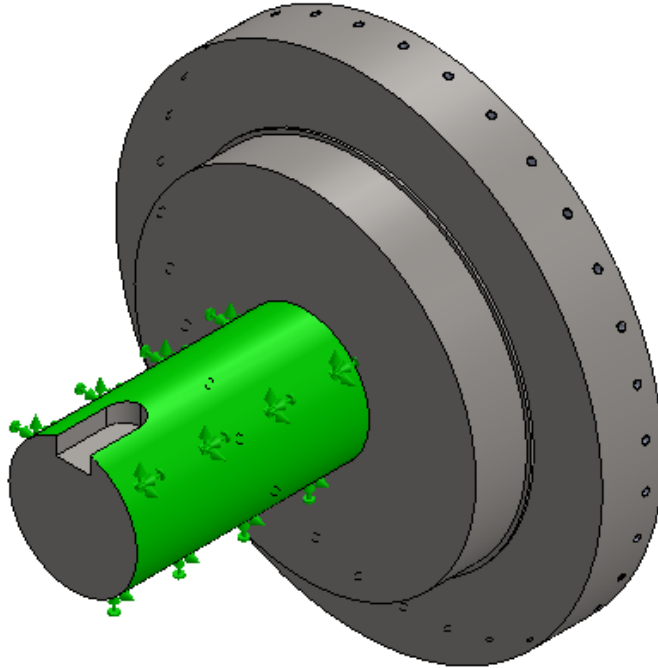


Figure 26: MG fixture example, fixed in three translational directions

3.4.5.6 Hybrid of FEA and Hand Calculation Method

There has been a hybrid method of FEA and hand/graphical calculations used in analyzing the gear which is focused on finite life. The finite life method used the Basquin's approximation formula for finite life where N is the number of cycles (27).

$$N = \left(\frac{\sigma_r}{A}\right)^{\frac{1}{B}} \quad (27)$$

Basquin's approximation formula requires subsequent formulas to complete the approximation; these are shown in (28) and (29), with a graphical example shown in Figure 27.

$$B = \frac{\log(\sigma_e) - \log(0.9\sigma_u)}{3} \quad (28)$$

$$A = \frac{\sigma_e}{10^{(6B)}} \quad (29)$$

The graphical example, shown in Figure 27, used an ultimate strength (σ_u) of 90000 psi and endurance limit (σ_e) of 40000 psi, while varying the applied stress load (σ_r). Use of these hand/graphical means to determine finite life was chosen due to the default FEA cyclical loading simulation results, which did not produce results that were applicable to this analysis. While using the Basquin approximation the maximum Von Mises Stress came from the simulations in SolidWorks, FEA plot shown in Figure 28.

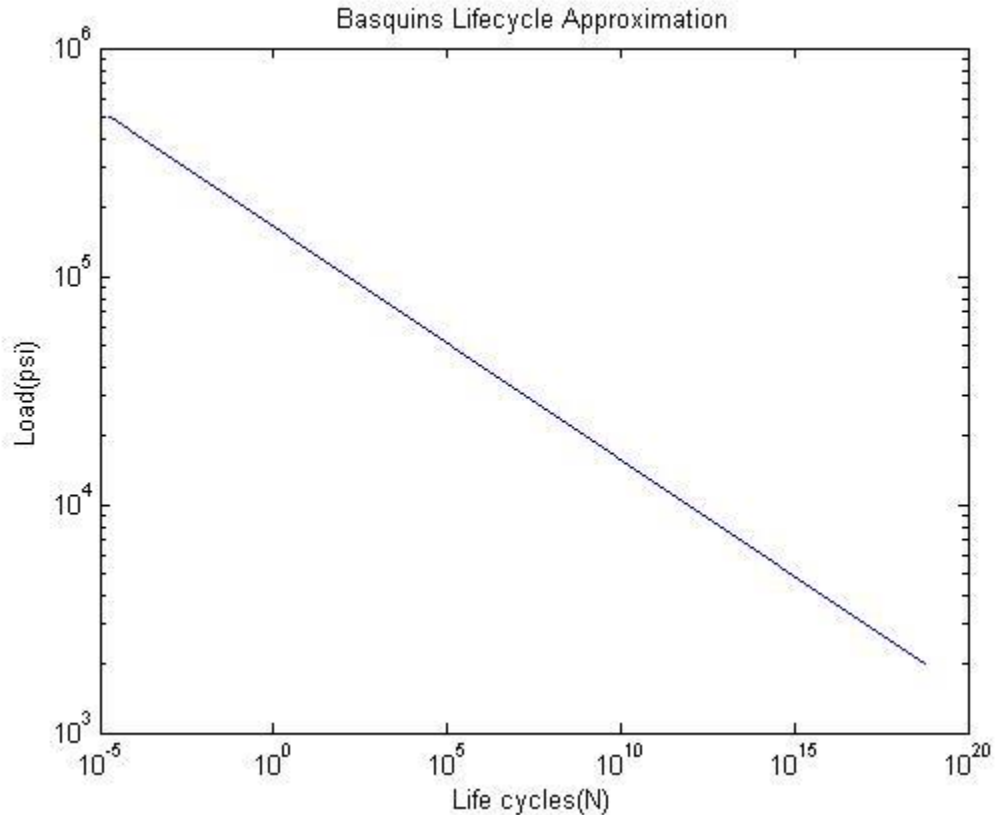


Figure 27: Basquin's life cycle approximation using an ultimate strength of 90000 psi and an endurance limit of 40000 psi while varying applied stress 'load'

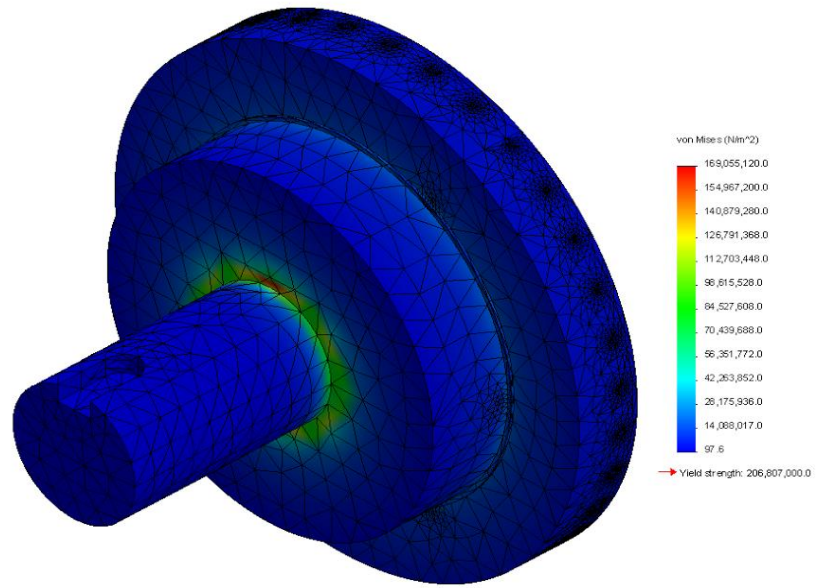


Figure 28: Radial magnetic gear FEA plot

3.4.5.7 Magnetic Gear Optimization

The MG optimization was completed by removing excess material in areas of low stress to lower the encompassing volume of the MG while also lowering the mass of the MG. By lowering the encompassing volume along with the mass of the MG, the MG becomes more competitive with the standard mechanical gearboxes. The optimization process was done by taking the previous simulations and removing excess material while still leaving the required support material and not allowing the Von Mises stress to increase to material failure of the part. After the optimization the Von Mises stress was then used to calculate the expected life of the part with cyclical loading. During these calculations there were no direct safety factors used due to the objective of the studies were to show where large amounts of excess material were removed. Although, there were indirect uses of safety factors during this analysis; this was done by rounding up forces, pressures and torques on all parts, i.e. 603 N/m^2 to 700 N/m^2 . This was done to

compensate for the fluctuation in loading on the parts at the given positions. With the results from this analysis highly excessive material was removed and the simulations were rerun under the same conditions. The optimized parts were then proposed for future work.

3.4.5.8 MG Mechanical Component Selection Analysis

The AFFMG's spoke rotor (center rotor) had an inner hub which had bolts that were specified with the assumption that the individual bars were simply supported beams, while also being verified for torque transmission requirements. This was later found to be untrue through the observation of the deflection of the bars along with the calculation of the deflection for a simply supported beam. It was calculated and observed that the bars could be more accurately modeled as cantilever beams. This was then experimentally verified by first measuring the no load deviation of the spoke rotor due to assembly and machining errors. These deviations were found to have some significance due to the slight inconsistency in the air-gap, which can increase the force on the given bar; the inconsistency can also cause greater torque ripple. The deviations show the spoke rotor with no-load; the measurements were made assuming the positive direction was in the opposite direction of the shaft in Figure 29, followed by the prototype component in Figure 30.

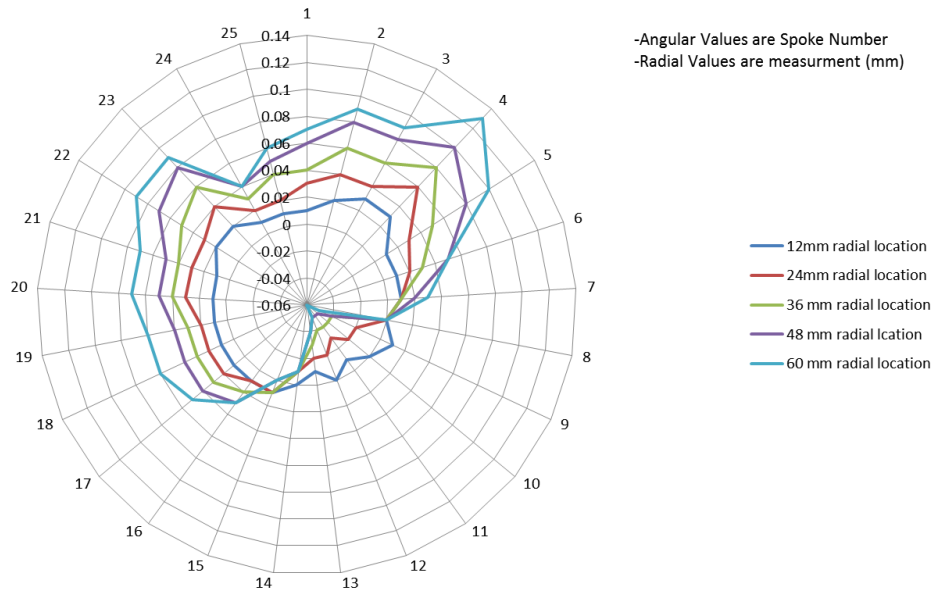


Figure 29: Axial MG spoke rotor no-load measurements showing deviations in assembly and machining



Figure 30: AFFMG prototype spoke rotor

The Axial MG's high speed and fixed rotor were then also measured to observe the assembly and machining deviations. These measurements showed very large deviations in the assembled rotors, which were a significant value of 0.2 mm. It was also observed that the fixed rotor to have a large deviation of up to 0.8 mm with a noticeable

trend to specific regions along the azimuthal direction, showing assembly and machining feature errors. These errors caused an increase in difficulty in maintaining a constant air-gap, which is crucial in the performance of a MG. The measurements for the Axial MG high speed and fixed rotor that were completed are shown the Figures 31 and 33, each of these are followed by their respective prototype component. These figures showed that each rotor had significant deviations. The fixed rotor data showed that bar 28 has very large deviation, this is most likely from machining errors.

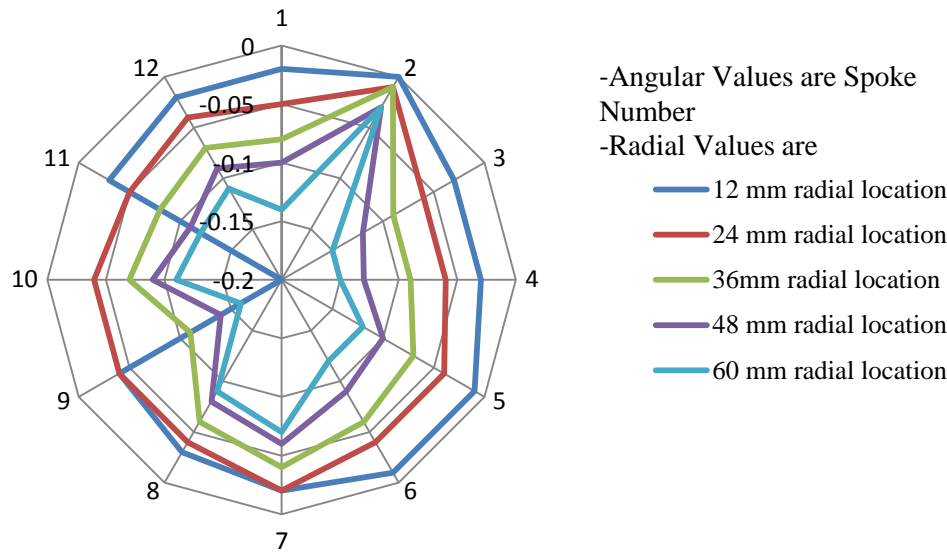


Figure 31: Axial MG high speed rotor deviation measurements



Figure 32: AFFMG prototype high speed rotor

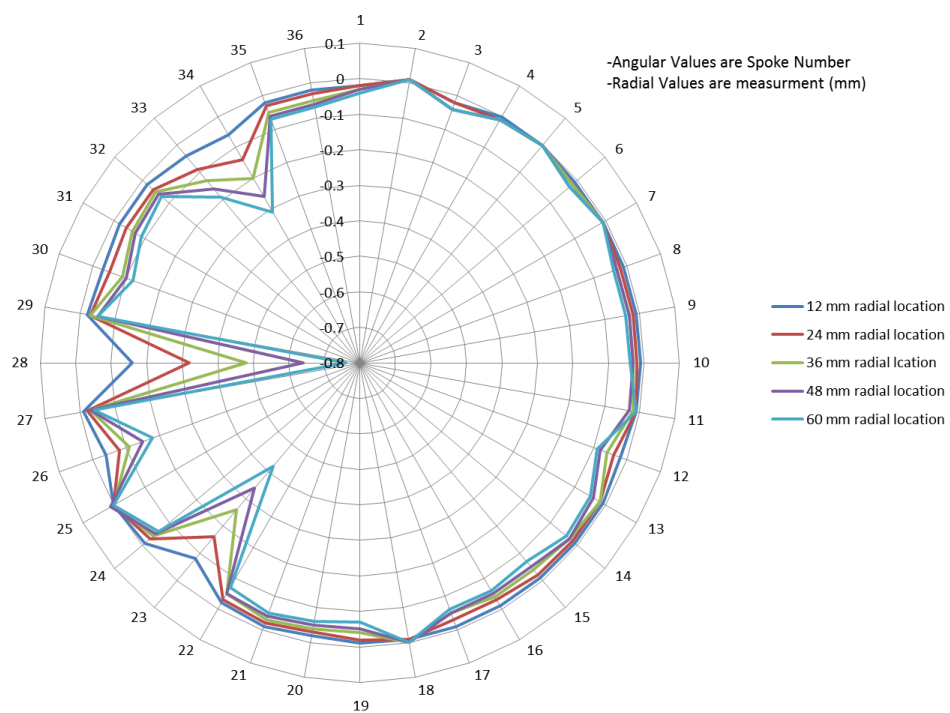


Figure 33: Axial MG fixed rotor deviation measurements



Figure 34: AFFMG prototype fixed rotor

The fixed rotor and the spoke rotor were then assembled with a series of shims that were designed to give an air-gap of 0.8 mm; after several trials of assembly this was determined to give an air-gap. Though this air-gap was inconsistent throughout the gearbox it was determined that the deviations and deflections needed to be measured. These measurements are shown in Figure 35; it shows a large deflection of the spoke rotor bars in the direction of the fixed rotor.

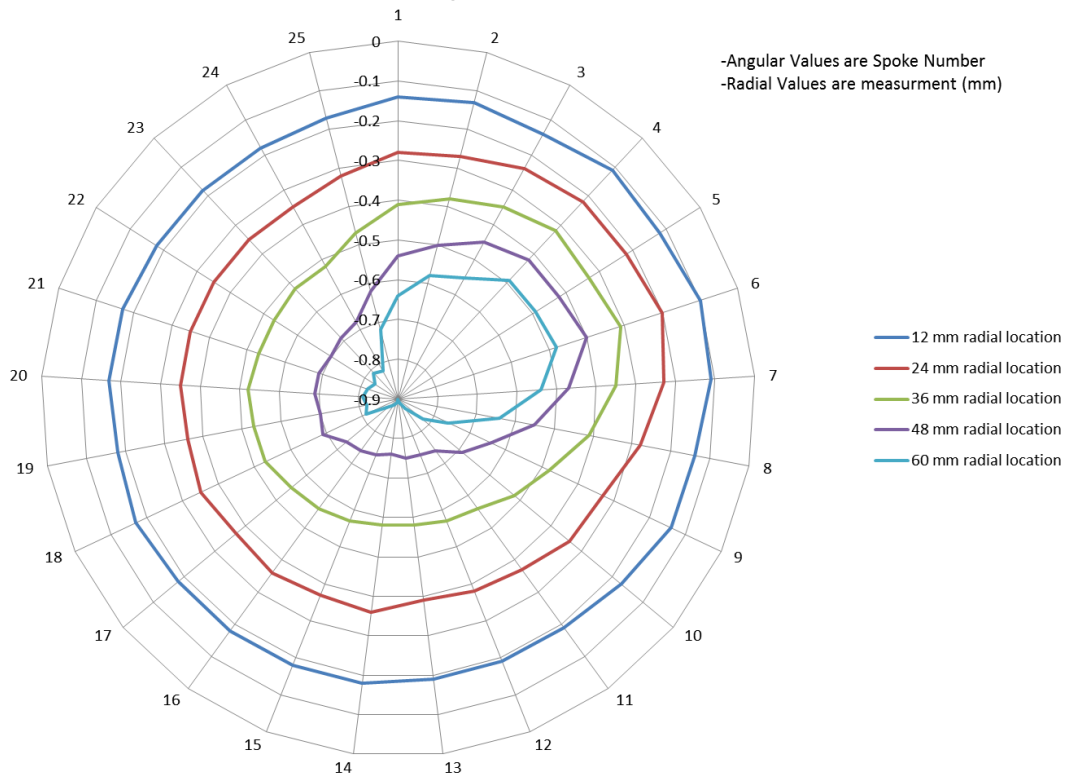


Figure 35: Axial MG spoke rotor uni-directionally loaded with the fixed rotor assembled together

From this information, it was determined that the bolts were deflecting which was causing a radial angular displacement. This caused a large air-gap change, greater than 0.2 mm, at the outer radius of the rotor. This information was then used to design a correction plate to compensate for the deflection. The correction plate design was then analyzed to determine the deflection that would be caused by the forces required to compensate for the deflection of the rotor. These deflections of the rotor were also experimentally measured and verified. The finalized correction pieces can be seen in Figure 36.

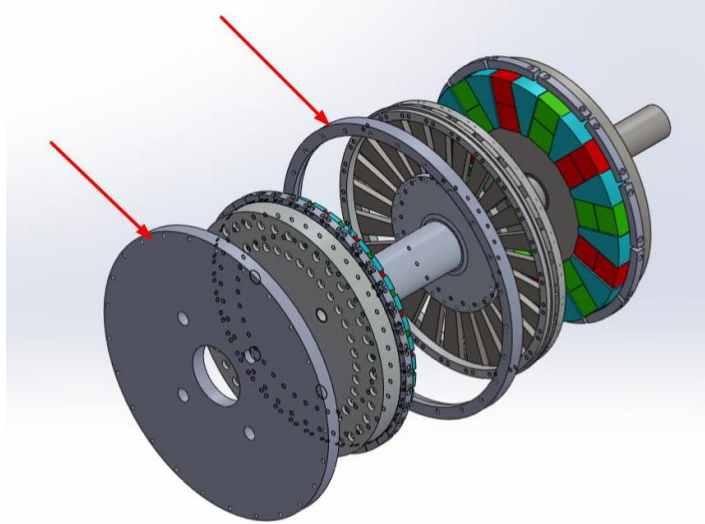


Figure 36: Axial MG including correction parts. The arrows are pointing to the correction plate and correction ring.

The FEA results showed a very small deflection in the axial direction as shown in the Figure 37. A static analysis was completed using one half of the total force experienced on the spoke rotor, which was previously generated from magnetic FEA simulations in JMAG. There was also a safety factor of 1.15 used along with material properties of AISI 316 sheet stainless steel.

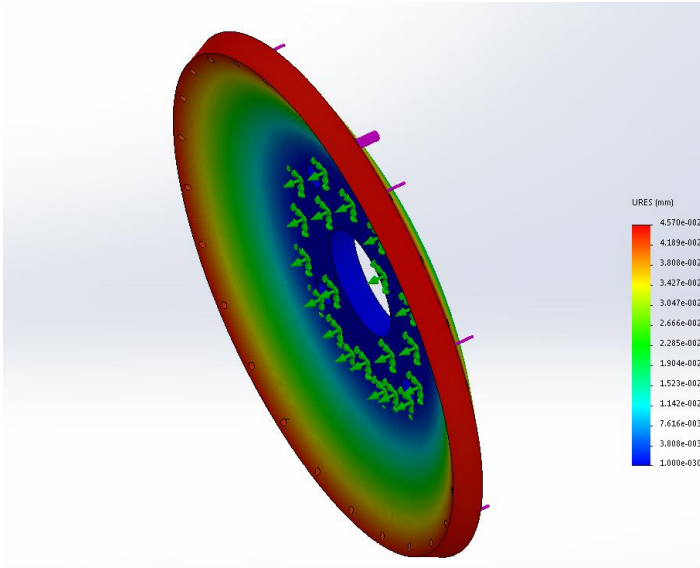


Figure 37: Deflection FEA of the correction plate

3.4.5.9 Axial Magnetic Gear Prototype Test Results

The prototype for the AFFMG had a gear ratio of 1:4.16. The AFFMG was found to have a peak torque of 546.2 Nm. This gave a volume torque density of 152 Nm/L and a specific torque density of 9.2 Nm/kg. The results also yielded a very low torque ripple through the AFFMG having a value of 2.5 Nm on the spoke rotor and a value of 5.5 Nm on the high speed rotor. The resulting torque densities are lower than predicted values from the JMAG simulations. Several possible reasons for the lower torque density include: an inconsistent air-gap, dimensional or tolerancing errors in the machining, magnetic volume error.

3.5 Expected Results

The goals for this project are to make a comparison of two types of gearboxes: standard mechanical and flux-focusing MG, in radial and axial configuration. The analysis completed on the AFFMG was to compare an AFFMG to previously proposed

and tested MGs, along with being able to compare the AFFMG to mechanical gearboxes. It was expected that this research would show that the AFFMG is comparable to the commonly used mechanical gearboxes in torque per unit mass and torque unit volume while having an inherent torque overload capability that does not have to be compensated for.

CHAPTER 4: RESULTS

4.1 Mechanical Gearbox

The mechanical gearboxes considered the comparison to the MGs are state-of-the-art gearboxes that are commercially available. The mechanical gearboxes analyzed were two different series of Nabtesco gearboxes (cycloidal 1 and cycloidal 2), analyzing each of the different sizes of gearboxes, as well as Sumitomo Cyclo inline reducer (cycloidal 3), two different series of Harmonic drive (Harmonic 1 and Harmonic 2), Planetgear (Planetary 1), Winsmith (Planetary 2). This was done to give a breadth of different types of gearboxes along with different manufacturers who will each have their own optimization process and their own limits due to optimization constraints. The volume torque densities (Nm/L) and specific torque densities (Nm/kg) are characterized by the diameter of gearboxes. The volume calculated was completed by excluding mounting features, bracketry, factory-installed couplings, shafts, etc. This was performed to remove all volume that is not required for torque transmission.

The torque that was used for the mechanical gearbox analysis was the rated torque. This was chosen due to the gearboxes being able to run constantly. There are peak torque specifications but those are for very short periods of time; they were dismissed due to not being an operation point for the gearboxes. The rated torque was then used to calculate the volume torque density (Nm/L). This has been chosen as the

primary method for analyzing the gearboxes while the secondary method for analyzing the gearboxes is the mass torque density or specific torque density (Nm/kg).

In Figure 38 and Figure 39 it is illustrated how the gearboxes were assumed to have a series of disks and how the dimensions were assigned over different features of the gearbox.

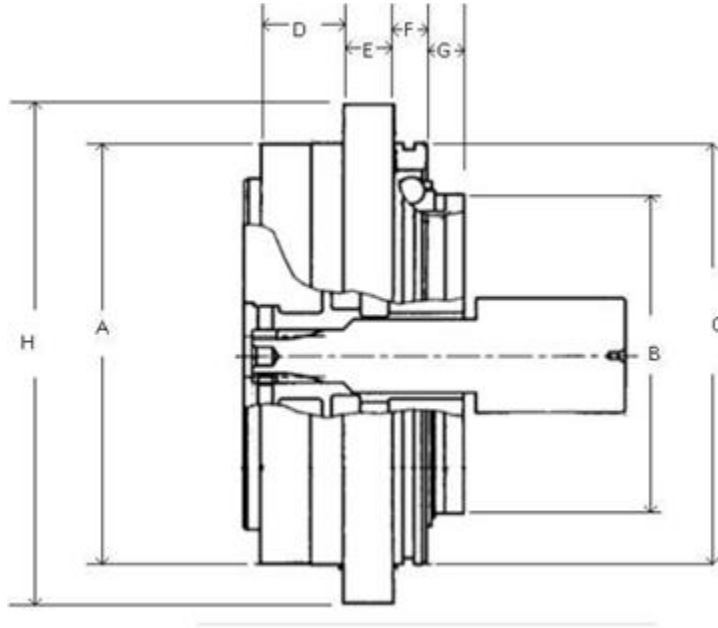


Figure 38: Cycloidal gearbox volume dimensions analysis example

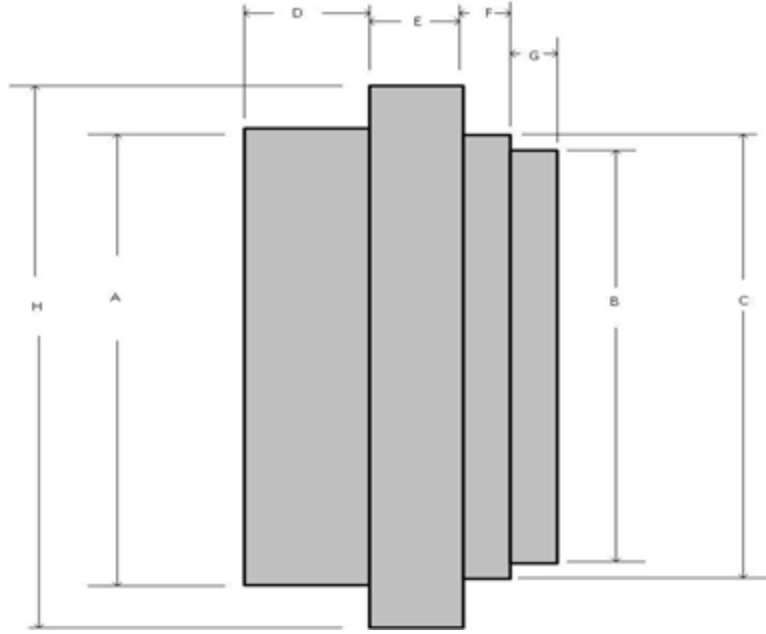


Figure 39: Cycloidal gearbox volume analysis cylinder diagram

4.1.1 Cycloidal Mechanical Gearbox

The analysis of the cycloidal gearboxes was done by taking the cycloidal gearbox data sheets for each of the different models and determining the region for the model that would be characterized as the active region. When looking at the torque density of the cycloidal gearboxes it showed that the torque density continued to rise from 320 mm to 400 mm diameter, then started to no longer increase the torque density. This is shown in both the specific torque density and the volume torque density. As shown in Figure 40 and 41 during the cycloidal torque density the actual radial MGs are comparable to several cycloidal gearboxes when looking at their torque density versus their given diameter size of the gearboxes. The scaled-up radial MG has a torque density of 235.8 Nm/L at a diameter of 228 mm while the higher perform cycloidal has a torque density of 300 Nm/L at a diameter of 240 mm. The scaled-up radial MG outperformed the

cycloidal gearbox that has a torque density of 195 Nm/L at a diameter of 230 mm. The specific torque density of the large scaled up MG at a specific torque density of 35.2 Nm/kg at a diameter of 228 mm fell between the cycloidal gearbox of 61.7 Nm/kg at a diameter of 222mm

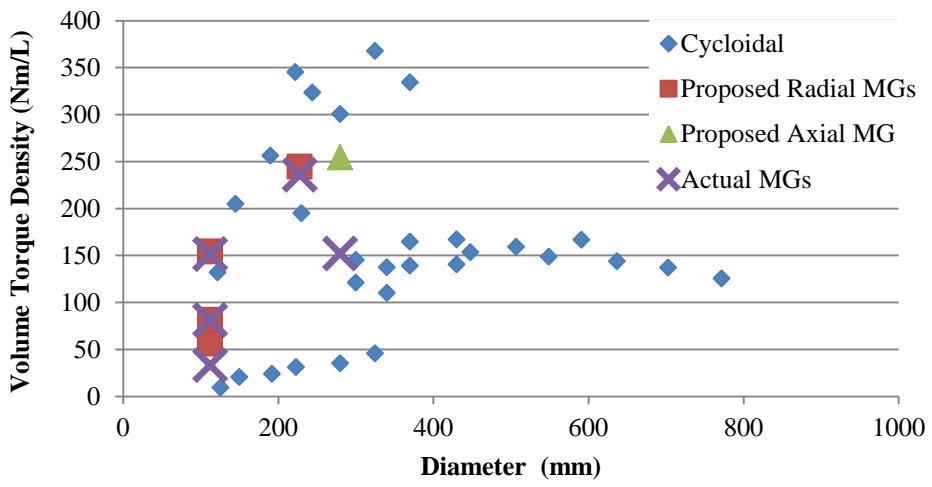


Figure 40: Cycloidal Volume torque density using active torque transfer region volume

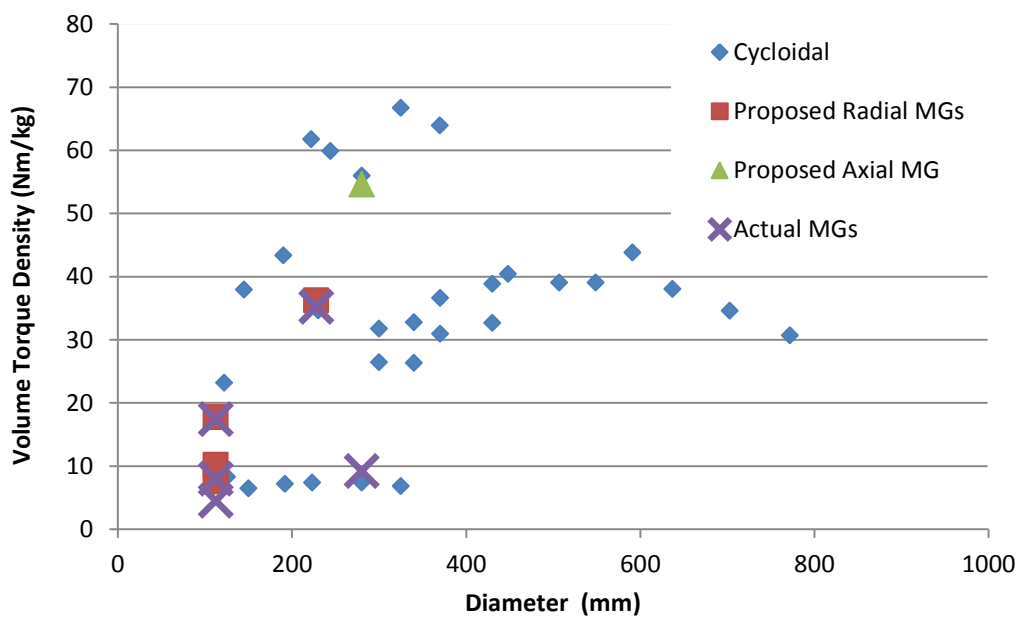


Figure 41: Cycloidal specific torque density using total mass of the gearbox

4.1.2 Harmonic Mechanical Gearbox

The Harmonic gearboxes tend to show a slight increasing torque density trend across ranging diameters. The plots show that the MGs are competitive with harmonic gearboxes when looking at both torque density by volume and specific torque density. These plots continue to confirm that the MGs are competitive with a variety of mechanical gearboxes, shown in Figure 42. The sub-scale rare earth radial MG has a torque density of 151.2 Nm/L at a diameter of 112 mm, this falls between two harmonic gearboxes one of which being at a volume torque density of 164 Nm/L at a diameter of 113 mm and 92.7 Nm/L at a diameter of 113 mm.

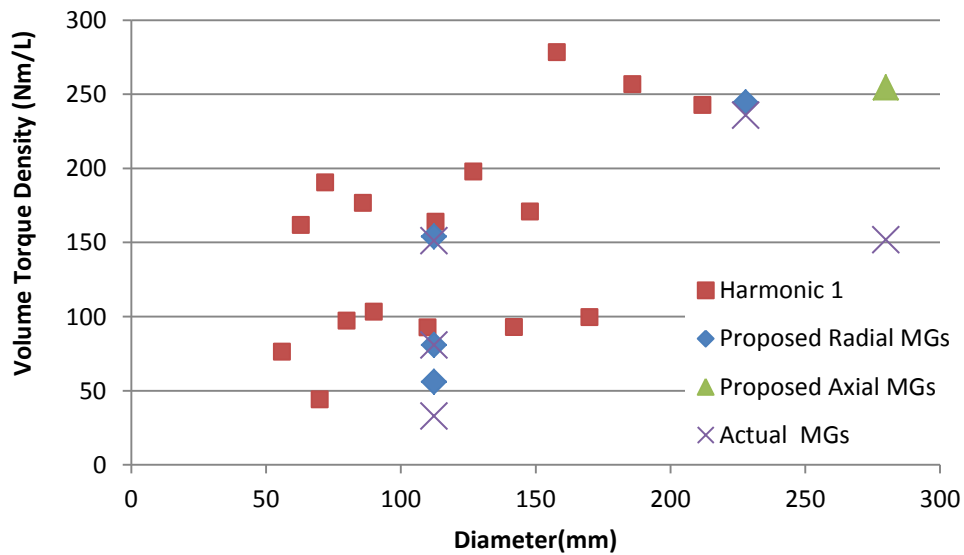


Figure 42: Harmonic gearbox volume torque density versus diameter including the comparison to the MGs

Figure 43, shows the specific torque density of the harmonic gearboxes versus the MGs. The data from Figure 43 confirms that the MGs are competitive with the harmonic gearboxes analyzed. The sub-scale radial MG has a torque density of 17.4 Nm/kg at a

diameter of 112 mm this falls between the harmonic gearboxes that have a specific torque density of 30.9 Nm/kg at a diameter of 113 mm and 17.4 Nm/kg at a diameter of 113mm.

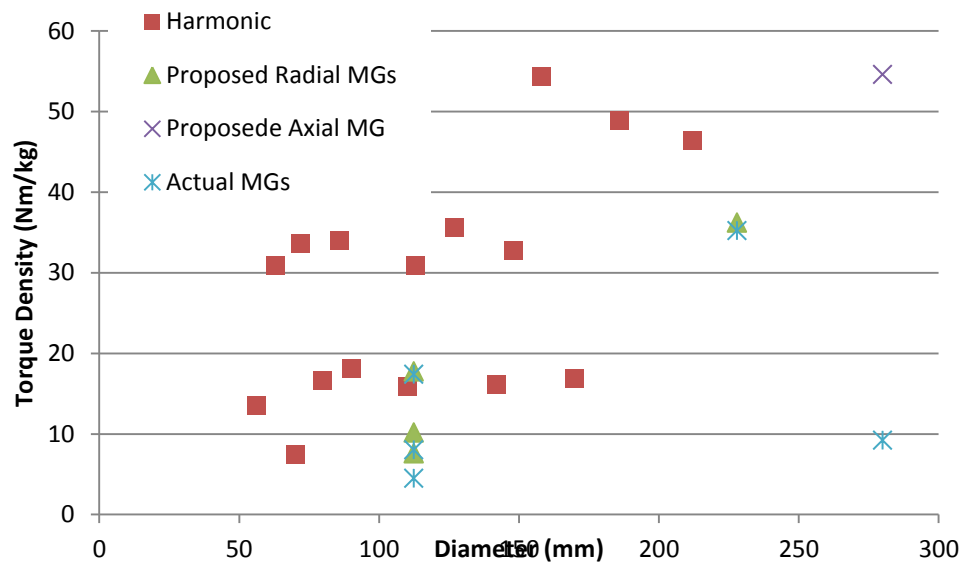


Figure 43: Harmonic gearbox specific torque density

4.1.3 Planetary Mechanical Gearbox

The planetary gearbox torque density did not increase as the diameter increased unlike the cycloidal, harmonic and MGs. From the range of gearboxes selected for the analysis, the MGs surpassed the torque density values in both the volume torque density and specific torque density, shown in Figures 44 and 45. The actual AFFMG surpassed the planetary gearboxes analyzed, having a torque density of 152 Nm/L at a diameter of 280 mm compared to the planetary of 77.3 Nm/L at a diameter of 267 mm. The specific torque density of the actual AFFMG at 9.2 Nm/kg at 280 mm fell between the planetary gearbox at 20.2 Nm/kg at a diameter of 267 mm and the planetary gearbox that had a specific torque density of 4.3 Nm/kg at a diameter of 293 mm. The planetary gearboxes tended to increase in torque density as the gear ratio increased until a point where there

was no longer a gain. This could have been caused by other limiting factors than the gear tooth limitations in the gearboxes.

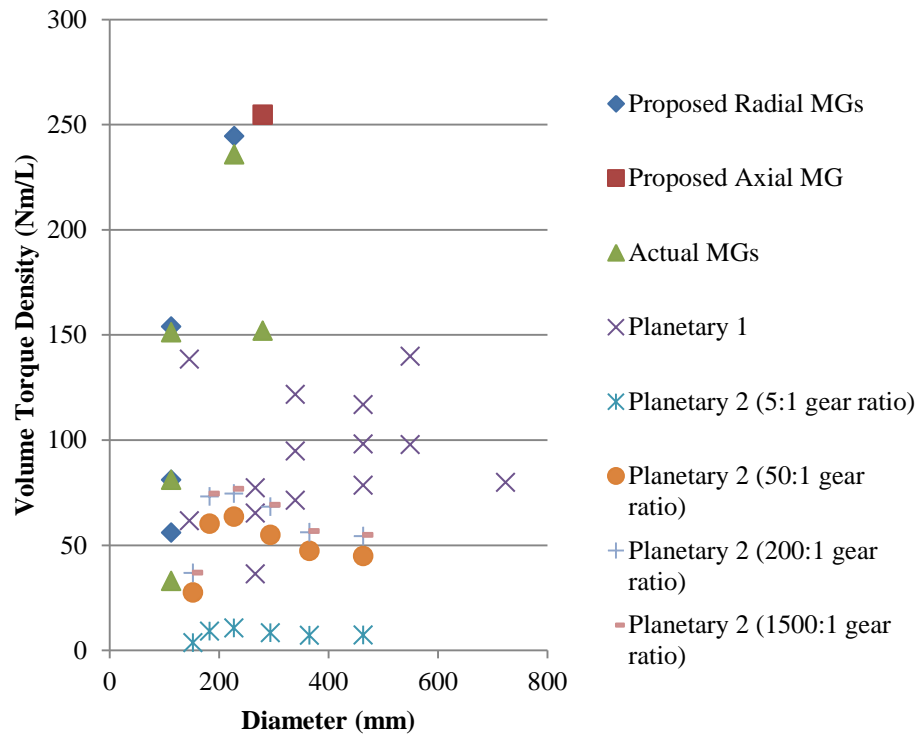


Figure 44: Planetary gearbox volume torque density including a variety of gear ratios

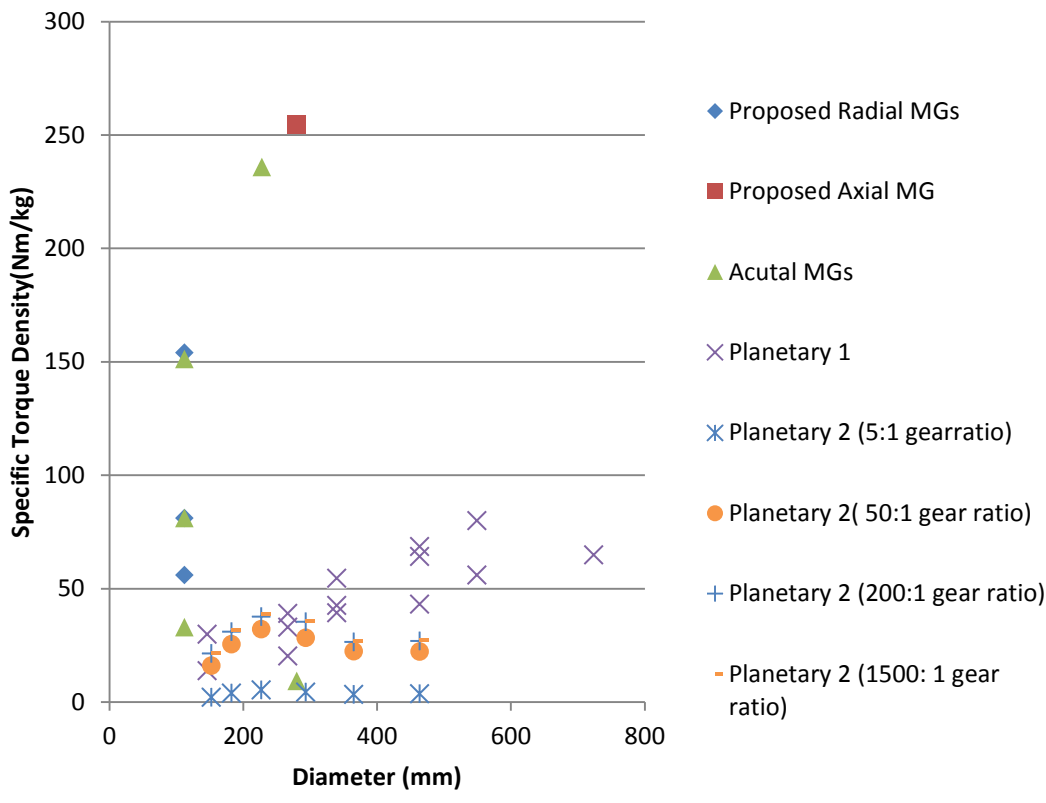


Figure 45: Planetary gearbox specific torque density including a variety of gear ratios

4.2 Magnetic Gearbox Testing

There have been several MGs tested during this research. The gearboxes tested are: a ferrite radial flux-focusing MG, neodymium radial flux-focusing MG, soft magnetic composite neodymium flux-focusing MG, lamination-neodymium radial flux-focusing MG, scaled up radial flux-focusing MG, and an AFFMG.

The radial flux-focusing MG previously tested showed an efficiency of greater than 97% for the designed speed of 20 RPM while even at five times the designed speed the radial flux-focusing MG shows an efficiency of greater than 92% while running at 100% of maximum load, shown in Figure 46. These efficiencies increased with a lower load percentage. These efficiencies at higher speeds can be increased by adding steel

laminations versus solid steel, which is currently being used. Using steel laminations reduces the eddy current losses that occur in solid steel components.

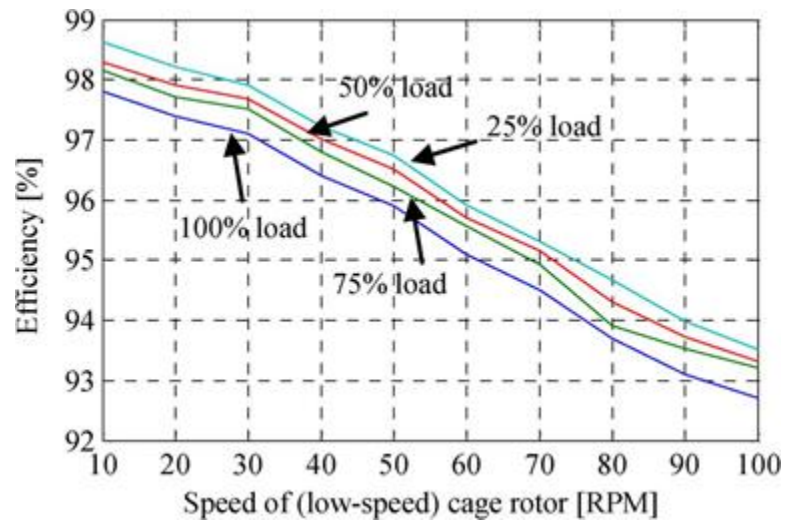


Figure 46: The efficiency plot of different loading percentages along with different operating speeds(K. K. Uppalapati et al., 2014)

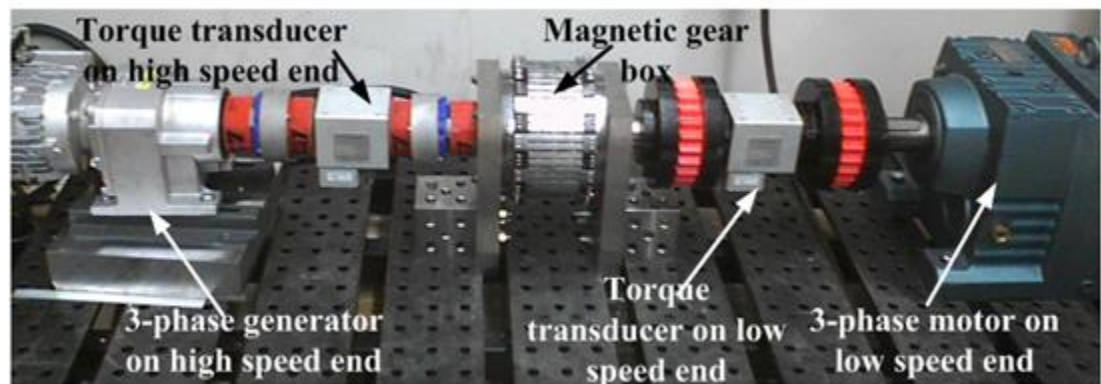


Figure 47: MG test setup. The test setup was used for the scaled up version of the radial gearbox and the axial gearbox (K. K. Uppalapati et al., 2014)

The AFFMG steel pole pieces were measured for machining and assembly errors, this was also used to assist in determining the deflection analysis of the rotors as detailed previously in chapter 3.

The efficiencies of AFFMG are shown in Figure 48, which shows an efficiency of greater than 96 % at the design operating speed of 20 RPM. While even at five times the designed speed the AFFMG shows an efficiency of greater than 91%. The test setup for the AFFMG prototype is shown in Figure 49. Where the torque is transmitted through a torque transducer then through the AFFMG, through another torque transducer into a generator and back into the power grid.

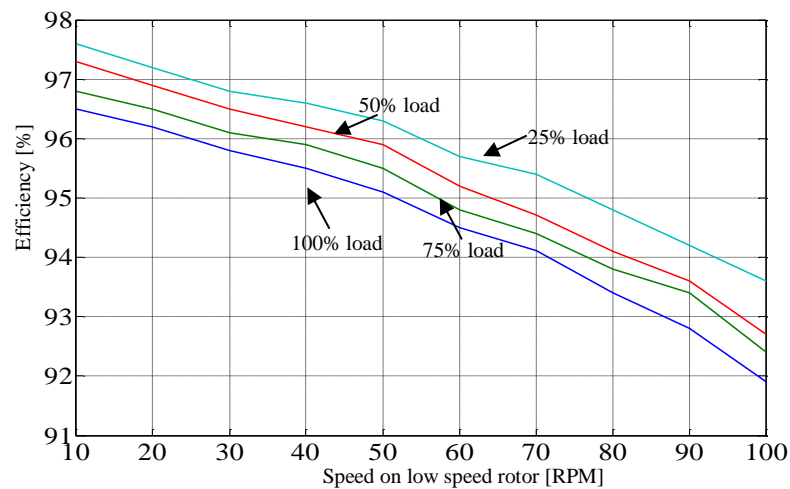


Figure 48: AFFMG prototype measured efficiency for different input speeds at different loading conditions

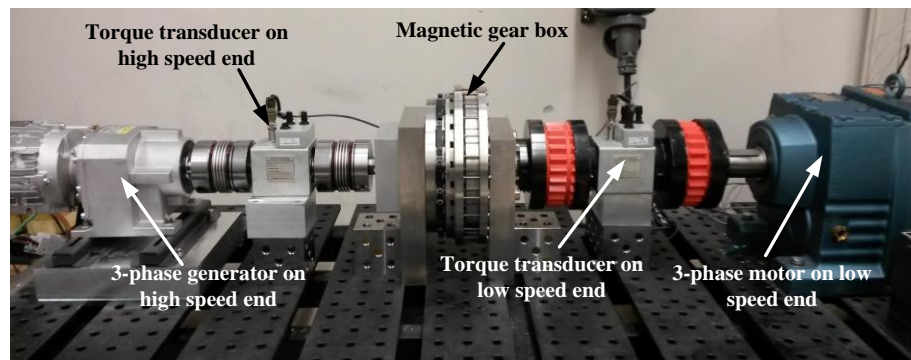


Figure 49: AFFMG prototype complete test bench setup

4.3 Summary of Results

- Two different MG topologies compared to three different topologies of mechanical gearboxes.
- MGs torque densities comparable to mechanical cycloidal gearboxes.
- MGs torque densities comparable to mechanical harmonic gearboxes.
- MGs torque densities comparable to mechanical planetary gearboxes.
- The forces in MGs require complete compensation in all directions.
- Mechanical features in MGs are still able to be optimized further from what has previously been done.

CHAPTER 5: CONCLUSION AND FUTURE SCOPE

5.1 Overview

In this thesis a comparison between two topologies of MGs and three topologies of mechanical gearboxes was performed. This was completed to give insight into applicability of MGs. This analysis showed the comparison of the active region of the MGs and the mechanical gearboxes; this is the region of the gearbox that is required for torque transfer. The method used for examining density of active regions is shown to be a viable method of comparison to the capabilities of each type of gearbox regardless of magnetic or mechanical or the topology of the gearboxes. It has been shown that the torque density of the active region of the MGs is comparable too mechanical gearboxes. This analysis indicated that the MGs' efficiency either meet or exceeded that of a mechanical counterpart that were compared. During the analysis it was also shown that as the MGs diameter increased the torque density also increased, resembling the pattern of the mechanical gearbox topologies. It should be noted that only low gear ratio MGs were considered in this comparison.

The difficulty in creating a prototype of an AFFMG was also studied. It was found that very high forces on the AFFMG components were present and it was not always possible to assume a fixed joint would continue to be fixed. Techniques to compensate for the component not being a fixed joint had to be developed. The

compensation for these difficulties was done by adding a correction plate and ring to mitigate a portion of the load from the previously assumed fixed joint.

A synopsis of the conclusions found in this paper are listed below:

- The performance comparison of several topologies of mechanical and MGs has been looked at for the first time.
- Two types of torque densities were presented. Torque density by volume (Nm/L) and torque density by mass (Nm/kg).
- The comparison of torque density by volume in this thesis showed that the MGs were competitive with a range of different mechanical gearboxes including cycloidal, harmonic and planetary. The comparison of torque density by mass tended to show the same results as the torque density by volume, with the exception of the AFFMG.
- When looking at the torque density by mass all of the gearboxes tended to have a very high increase in torque density as diameter increased whereas when looking at the torque density by volume, with the exception of cycloidal 3 and Planetary 1, they did not increase as rapidly when looking at torque density by volume.
- The MGs while looking at torque density stayed grouped with the higher performing gearboxes regardless of diameter or method.
- The difficulties of prototype assembly and design were investigated and it showed that the tolerances should be kept small to continue to better match that of a production mechanical gearbox.

5.2 Recommendations and Future Scope

A larger range of mechanical gearboxes should be considered for future work with a focus on larger scale gearboxes that are used for energy applications to match the current work on larger scale MGs. Other low impact conditions should also be considered for a further comparison of MG, such as large earth moving equipment or coupled with electric motors. Observing gearboxes both mechanical and magnetic that have the same gear ratio along with the same torque capabilities should be considered for future work. A more rigorous analysis on efficiency across different loading characteristics throughout a larger rotational speed range is recommended for future work.

The analysis presented in the test can be extended to other MG topologies as a standard method of comparison for all MGs and mechanical gearboxes. In the thesis, the difficulties of each type of gearbox were presented as an equivalency analysis that should be considered for expansion of this topic. A section on the difficulties of each type of gearbox can be done by completing a failure mode analysis of each topology of gearboxes.

The methods presented in this thesis can be also be used to compare efficiencies with different diameters at a given speed. This can then be overlaid on a torque density by volume or torque density by mass plot. This should also be considered at different load percentages to give a more complete idea on how the gearboxes compare to each other.

An expansion of deflection analysis for each of the components of a MG should be analyzed with more detail. The forces of a MG should be further studied with variable

air-gaps; this should be done due to the oscillatory nature of the MGs. The oscillatory forces can cause vibrations through-out the system which can degrade the lifetime of the system; if this can be controlled the lifetime of the system could increase. Further life cycle analysis for each MG should be considered to determine the theoretical life cycle of the MG. This should be done along with the methods of testing lift time over a shorter period of time much like what is done for determining lifetime of mechanical gearboxes.

REFERENCES

- Acharya, V. M. (2013). *Design of a flux focusing axial magnetic gear*. Available from <http://worldcat.org/z-wcorg/database>.
- Acharya, V. M., Bird, J. Z., & Calvin, M. (2013). A Flux Focusing Axial Magnetic Gear. *Magnetics, IEEE Transactions on*, 49(7), 4092-4095. doi: 10.1109/TMAG.2013.2248703
- Acharya, V. M., Calvin, M., & Bird, J. Z. (2014, 8-10 April 2014). *A low torque ripple flux focusing axial magnetic gear*. Paper presented at the Power Electronics, Machines and Drives (PEMD 2014), 7th IET International Conference on.
- Bronn, L. (2012). *Design and performance evaluation of a magnetically geared axial-flux permanent magnet generator*. Stellenbosch: Stellenbosch University.
- Cheng-Chi, H., Mi-Ching, T., Dorrell, D. G., & Bor-Jeng, L. (2008). Development of a Magnetic Planetary Gearbox. *Magnetics, IEEE Transactions on*, 44(3), 403-412. doi: 10.1109/TMAG.2007.914665
- Corey, C. A. (2003). Epicyclic Gear train Solution Techniques with application to tandem bicycling.
- Crowder, R. M. (2006). Electric drives and electromechanical systems. from <http://search.ebscohost.com/login.aspx?direct=true&scope=site&db=nlebk&db=nlabk&AN=195109>
- Faus, H. T. (1941). Magnet gearing: Google Patents.
- Frank, N. W. (2011). Analysis of The Concentric Planetary magnetic gear.
- Gouda, E., Mezani, S., Baghli, L., & Rezzoug, A. (2011). Comparative Study Between Mechanical and Magnetic Planetary Gears. *Magnetics, IEEE Transactions on*, 47(2), 439-450. doi: 10.1109/TMAG.2010.2090890
- Hesmondhalgh, D. E., & Tipping, D. (1980). A multielement magnetic gear. *Electric Power Applications, IEE Proceedings B*, 127(3), 129-138. doi: 10.1049/ip-b:19800017

- Litvin, F. L., & Lewis Research, C. (1997). *Development of gear technology and theory of gearing*. [Cleveland, Ohio]; Springfield, Va.: National Aeronautics and Space Administration, Lewis Research Center ; National Technical Information Service, distributor.
- Maiti, R. (2004). A novel harmonic drive with pure involute tooth gear pair. *Journal of Mechanical Design*, 126(1), 178-182.
- MatWeb. (3/13/15). [material database] Retrieved from <http://www.matweb.com/>
- Mobley, R. K. (1999). Root cause failure analysis. from <http://site.ebrary.com/id/10206658>
- Neuland, A. H. (1916). Apparatus for transmitting power: Google Patents.
- Nikolaus, L. (1972). Magnetic transmission: Google Patents.
- Operating Principles. (2015, 2015). Retrieved 5/5/2015, 2015, from <http://harmonicdrive.net/reference/operatingprinciples/>
- Oyague, F. (2009). Gearbox Modeling and Load Simulation of a Baseline 750-kW-Wind Turbine Using State-of-the-Art Simulation Codes. Golden, Colorado: National Renewable Energy Laboratory.
- Ragheb, A., & Ragheb, M. (2010). *Wind turbine gearbox technologies*. Paper presented at the Nuclear & Renewable Energy Conference (INREC), 2010 1st International.
- Reese, G. A. (1967). Magnetic gearing arrangement: Google Patents.
- Regan, S. (1895). Power-transmitter: Google Patents.
- Sensinger, J. W. (2010). Unified approach to cycloid drive profile, stress, and efficiency optimization. *Journal of Mechanical Design*, 132(2), 024503.
- Shin, J.-H., & Kwon, S.-M. (2006). On the lobe profile design in a cycloid reducer using instant velocity center. *Mechanism and Machine Theory*, 41(5), 596-616. doi: <http://dx.doi.org/10.1016/j.mechmachtheory.2005.08.001>

- Spotts, M. F., Shoup, T. E., Hornberger, L. E., & Kazmer, D. O. (2004). Design of Machine Elements, Eighth Edition. *J. Mech. Des. Journal of Mechanical Design*, 126(1), 201.
- Tan, C. K., Irving, P., & Mba, D. (2007). A comparative experimental study on the diagnostic and prognostic capabilities of acoustics emission, vibration and spectrometric oil analysis for spur gears. *Mechanical Systems and Signal Processing*, 21(1), 208-233. doi: <http://dx.doi.org/10.1016/j.ymssp.2005.09.015>
- Thomas, M. B. (1968). Magnetic transmission: Google Patents.
- Tsurumoto, K., & Kikuchi, S. (1987). A new magnetic gear using permanent magnet. *Magnetics, IEEE Transactions on*, 23(5), 3622-3624. doi: 10.1109/TMAG.1987.1065208
- Ueura, K., & Slatter, R. (1999). Development of the harmonic drive gear for space applications. *EUROPEAN SPACE AGENCY-PUBLICATIONS-ESA SP*, 438, 259-264.
- Uppalapati, K., & Bird, J. (2012, 27-29 March 2012). *A flux focusing ferrite magnetic gear*. Paper presented at the Power Electronics, Machines and Drives (PEMD 2012), 6th IET International Conference on.
- Uppalapati, K. K., Bird, J. Z., Dan, J., Garner, J., & Zhou, A. (2012, 15-20 Sept. 2012). *Performance of a magnetic gear using ferrite magnets for low speed ocean power generation*. Paper presented at the Energy Conversion Congress and Exposition (ECCE), 2012 IEEE.
- Uppalapati, K. K., Bird, J. Z., Wright, J., Pitchard, J., Calvin, M., & Williams, W. (2014, 14-18 Sept. 2014). *A magnetic gearbox with an active region torque density of 239Nm/L*. Paper presented at the Energy Conversion Congress and Exposition (ECCE), 2014 IEEE.
- Weisstein, E. Involute. from <http://mathworld.wolfram.com/Involute.html>

APPENDIX: GEARBOX RAW DATA

| Magnetic Gears | Diameter(mm) | Torque (Nm) | Torque Density(Nm/L) | Mass (kg) | Specific Torque Density(Nm/kg) |
|--|---------------------|--------------------|-----------------------------|------------------|---------------------------------------|
| Proposed Axial Flux Focusing Magnetic Gear | 280.0 | 830.3 | 254.7 | 14.99 | 54.6 |
| Proposed Small Scale Radial Flux Focusing Magnet Gear(Ferrite) | 112.4 | 42.0 | 56.0 | 5.6 | 7.6 |
| Proposed Small Scale Radial Flux Focusing Magnet Gear(Hybrid) | 112.4 | 61.0 | 81.0 | 6.0 | 10.2 |
| Proposed Small Scale Radial Flux Focusing Magnet Gear(NdFeB) | 112.4 | 115.7 | 154.0 | 6.5 | 17.7 |
| Proposed Scaled up Radial Flux Focusing Magnetic Gear | 228.0 | 750.0 | 244.5 | 20.7 | 36.2 |
| Actual Scaled up Radial Flux Focusing Magnetic Gear | 228.0 | 731.0 | 235.8 | 20.8 | 35.2 |
| Actual Small Scale Radial Flux Focusing Magnet Gear(Ferrite) | 112.4 | 25.0 | 33.0 | 5.6 | 4.5 |
| Actual Small Scale Radial Flux Focusing Magnet Gear(Hybrid) | 112.4 | 48.0 | 81.0 | 6.0 | 8.0 |
| Actual Small Scale Radial Flux Focusing Magnet Gear(NdFeB) | 112.4 | 113.5 | 151.2 | 6.5 | 17.4 |
| Actual Axial Flux Focusing Magnetic Gear (NdFeB) | 280.0 | 546.2 | 152 | 56 | 9.7 |

| Cycloidal Mechanical Gearboxes | Model | Diameter (mm) | Torque (Nm) | Torque Density (Nm/L) | Mass(kg) | Specific Torque Density (Nm/kg) |
|---|--------------|----------------------|--------------------|------------------------------|-----------------|--|
| Nabtesco | RD-E006e | 125.5 | 58.0 | 9.2 | 6.3 | 8.3 |
| Cycloidal 1 | RD-E020e | 150.0 | 167.0 | 20.4 | 8.2 | 6.5 |
| | RD-E040e | 192.0 | 412.0 | 23.8 | 17.3 | 7.2 |
| | RD-E080E | 223.0 | 784.0 | 31.1 | 25.2 | 7.4 |
| | RD-E160E | 280.0 | 1568.0 | 35.2 | 44.5 | 7.4 |
| | RD-E320E | 325.0 | 3136.0 | 45.6 | 68.7 | 6.8 |
| Cycloidal 2 | RV-E6E | 122.0 | 58.0 | 131.9 | 2.5 | 23.2 |
| | RV-E20E | 145.0 | 167.0 | 204.9 | 4.4 | 38.0 |
| | RV-E40E | 190.0 | 412.0 | 256.1 | 9.5 | 43.4 |
| | RV-E80E | 222.0 | 784.0 | 345.1 | 12.7 | 61.7 |
| | RV-E110E | 244.0 | 1078.0 | 323.4 | 18.0 | 59.9 |
| | RV-E160E | 280.0 | 1568.0 | 300.5 | 28.0 | 56.0 |
| | RV-E320 | 325.0 | 3136.0 | 367.8 | 47.0 | 66.7 |
| | RV-E450E | 370.0 | 4410.0 | 334.2 | 69.0 | 63.9 |
| Sumitomo Drive Technologies Cyclo 6000 series | 6145 | 230.1 | 1288.0 | 195.1 | 37.2 | 34.6 |
| Cycloidal 3 | 6160 | 300.0 | 1751.3 | 121.0 | 66.2 | 26.4 |
| | 6165 | 300.0 | 2101.5 | 145.2 | 66.2 | 31.7 |
| | 6170 | 340.1 | 2530.9 | 110.1 | 96.2 | 26.3 |
| | 6175 | 340.1 | 3152.3 | 137.2 | 96.2 | 32.8 |
| | 6180 | 370.1 | 4056.2 | 139.0 | 131.1 | 30.9 |
| | 6185 | 370.1 | 4801.9 | 164.6 | 131.1 | 36.6 |
| | 6190 | 430.0 | 6372.3 | 140.5 | 195.0 | 32.7 |
| | 6195 | 430.0 | 7581.3 | 167.1 | 195.0 | 38.9 |
| | 6205 | 448.1 | 8620.7 | 153.5 | 213.2 | 40.4 |
| | 6215 | 507.0 | 11411.5 | 159.0 | 292.1 | 39.1 |
| | 6225 | 548.9 | 13558.2 | 148.7 | 347.0 | 39.1 |
| | 6235 | 591.1 | 18755.5 | 166.8 | 428.2 | 43.8 |
| | 6245 | 637.0 | 20450.3 | 143.9 | 538.0 | 38.0 |
| | 6255 | 703.1 | 27455.3 | 137.2 | 794.2 | 34.6 |
| | 6265 | 771.9 | 31296.8 | 125.5 | 1020.1 | 30.7 |

| Harmonic Mechanical Gearboxes | Model | Diameter (mm) | Torque (Nm) | Torque Density (Nm/L) | Mass(kg) | Specific Torque Density (Nm/kg) |
|--------------------------------------|----------------|----------------------|--------------------|------------------------------|-----------------|--|
| Harmonic Drive | csd-40-xxx-2uf | 170.0 | 96.0 | 99.7 | 5.7 | 16.8 |
| Harmonic 1 | csd-32-xxx-2uf | 142.0 | 53.0 | 93.0 | 3.3 | 16.1 |
| | csd-25-xxx-2uf | 110.0 | 27.0 | 92.8 | 1.7 | 15.9 |
| | csd-20-xxx-2uf | 90.0 | 17.0 | 103.4 | 0.9 | 18.1 |
| | csd-17-xxx-2uf | 80.0 | 11.0 | 97.4 | 0.7 | 16.7 |
| | csd-14-xxx-2uf | 70.0 | 3.7 | 44.2 | 0.5 | 7.4 |
| Harmonic 2 | csg-14-2uh | 56.0 | 7.0 | 76.4 | 0.5 | 13.5 |
| | CSG-17-2uh | 63.0 | 21.0 | 161.8 | 0.7 | 30.9 |
| | CSG-20-2uh | 72.0 | 33.0 | 190.5 | 1.0 | 33.7 |
| | csg-25-2uh | 86.0 | 51.0 | 176.9 | 1.5 | 34.0 |
| | csg-32-2uh | 113.0 | 99.0 | 164.1 | 3.2 | 30.9 |
| | csg-40-2uh | 127.0 | 178.0 | 197.9 | 5.0 | 35.6 |
| | csg-45-2uh | 148.0 | 229.0 | 171.0 | 7.0 | 32.7 |
| | csg-50-2uh | 158.0 | 484.0 | 278.5 | 8.9 | 54.4 |
| | csg-58-2uh | 186.0 | 714.0 | 256.9 | 14.6 | 48.9 |
| | csg-65-2uh | 212.0 | 969.0 | 242.9 | 20.9 | 46.4 |

| Planetary Mechanical Gearboxes | Model | Diameter (mm) | Torque (Nm) | Torque Density (Nm/L) | Mass(kg) | Specific Torque Density (Nm/kg) |
|---------------------------------------|--------------|----------------------|--------------------|------------------------------|-----------------|--|
| Rexnord | 7200 | 146.1 | 903.9 | 61.5 | 65.5 | 13.8 |
| Planetary 1 | 7220 | 146.1 | 2033.7 | 138.5 | 68.2 | 29.8 |
| | 7240 | 266.7 | 2711.6 | 36.4 | 134.1 | 20.2 |
| | 7260 | 266.7 | 4858.3 | 65.2 | 147.7 | 32.9 |
| | 7280 | 266.7 | 5762.2 | 77.3 | 147.7 | 39.0 |
| | 7300 | 339.7 | 8586.8 | 71.4 | 218.6 | 39.3 |
| | 7320 | 339.7 | 13558.2 | 94.8 | 319.1 | 42.5 |
| | 7340 | 339.7 | 17399.7 | 121.7 | 319.1 | 54.5 |
| | 7360 | 463.6 | 18077.6 | 78.5 | 419.6 | 43.1 |
| | 7380 | 463.6 | 26890.4 | 116.8 | 419.6 | 64.1 |
| | 7400 | 463.6 | 35703.2 | 98.0 | 520.9 | 68.5 |
| | 7420 | 549.3 | 50843.2 | 97.9 | 909.1 | 55.9 |
| | 7440 | 549.3 | 72649.2 | 139.8 | 909.1 | 79.9 |
| 7460 | 723.9 | 102251.3 | 79.8 | 1577.3 | 64.8 | |
| Winsmith | 1r | 152.4 | 26.4 | 3.6 | 12.7 | 2.1 |
| Planetary 2 | 10r | 182.6 | 78.5 | 9.1 | 20.5 | 3.8 |
| | 20r | 227.0 | 181.6 | 10.5 | 34.1 | 5.3 |
| | 30r | 293.7 | 294.8 | 8.4 | 68.2 | 4.3 |
| | 40r | 365.1 | 453.7 | 7.0 | 136.4 | 3.3 |
| | 50r | 463.6 | 943.8 | 7.3 | 261.4 | 3.6 |
| | 1r | 152.4 | 203.4 | 27.4 | 12.7 | 16.0 |
| | 10r | 182.6 | 521.0 | 60.3 | 20.5 | 25.5 |
| | 20r | 227.0 | 1095.5 | 63.6 | 34.1 | 32.1 |
| | 30r | 293.7 | 1934.2 | 54.8 | 68.2 | 28.4 |
| | 40r | 365.1 | 3051.6 | 47.3 | 136.4 | 22.4 |
| | 50r | 463.6 | 5808.9 | 44.8 | 261.4 | 22.2 |
| | 1r | 152.4 | 272.9 | 36.8 | 12.7 | 21.4 |
| | 10r | 182.6 | 632.7 | 73.2 | 20.5 | 30.9 |
| | 20r | 227.0 | 1283.7 | 74.5 | 34.1 | 37.7 |
| | 30r | 293.7 | 2406.6 | 68.2 | 68.2 | 35.3 |
| | 40r | 365.1 | 3615.5 | 56.1 | 136.4 | 26.5 |
| | 50r | 463.6 | 7031.0 | 54.2 | 261.4 | 26.9 |
| | 1r | 152.4 | 274.0 | 37.0 | 12.7 | 21.5 |
| | 10r | 182.6 | 644.0 | 74.5 | 20.5 | 31.5 |
| | 20r | 227.0 | 1321.9 | 76.8 | 34.1 | 38.8 |
| | 30r | 293.7 | 2440.5 | 69.2 | 68.2 | 35.8 |
| | 40r | 365.1 | 3660.7 | 56.8 | 136.4 | 26.8 |
| | 50r | 463.6 | 7118.0 | 54.9 | 261.4 | 27.2 |